

Estimating the Satellite Equatorial Crossing Time Biases in the Daily, Global Outgoing Longwave Radiation Dataset

L. E. LUCAS AND D. E. WALISER

Institute for Terrestrial and Planetary Atmospheres, State University of New York, Stony Brook, Stony Brook, New York

P. XIE AND J. E. JANOWIAK

Climate Prediction Center/NCEP/NWS/NOAA, Camp Springs, Maryland

B. LIEBMANN

Climate Diagnostics Center, University of Colorado, Boulder, Colorado

(Manuscript received 22 February 2000, in final form 13 September 2000)

ABSTRACT

Due to its long record length (approximately 25 years), the outgoing longwave radiation (OLR) dataset has been used in a multitude of climatological studies including studies on tropical circulation and convection, the El Niño–Southern Oscillation (ENSO) phenomenon, and the earth's radiation budget. Although many of the climatological studies using OLR have proven invaluable, proper interpretation of the low-frequency components of the data could be limited by the presence of biases introduced by changes in the satellite equatorial crossing time (ECT). Since long-term global changes could be masked or contaminated by this instrumental bias, it is necessary to take steps to ensure that the daily, global OLR dataset is free from such biases and is as accurate as possible.

The goal of this study is to derive a method for estimating the ECT biases in the daily, global OLR dataset. Our analysis utilizes a Procrustes targeted empirical orthogonal function rotation (REOF) on an interpolated OLR dataset to try to isolate and remove the two major ECT biases—afternoon satellite orbital drift and the abrupt transitions from a morning satellite to an afternoon satellite—from the dataset. Two targeted REOF analyses are performed to separate and distinguish between these two artificial satellite bias modes. A “common ECT” of approximately 0245 LST is established for the dataset by removing an estimate of these two ECT biases.

Results from the analysis indicate that changes in ECTs can cause large regional biases over both ocean and tropical landmasses. The afternoon satellite ECT drift-bias accounts for 0.4% of the pentad anomaly variance. During a single satellite series (e.g., *NOAA-11*), the afternoon drift-bias can introduce a difference as large as 10.5 W m^{-2} in the OLR values collected over most tropical landmasses. The morning to afternoon satellite transition bias accounts for 0.9% of the pentad anomaly variance, and is shown to cause a bias of 12 W m^{-2} in the OLR values over most tropical landmasses during the NOAA-SR satellite series. The data are corrected by removing a statistically derived synthetic eigenvector that is associated with each of the ECT bias modes. This synthetic eigenvector is used instead of the exact values of the satellite bias eigenvector to ensure that only the artificial variability is removed from the dataset.

The two REOF modes produced in this study are nearly orthogonal to each other having a correlation of only 0.17. This near orthogonality suggests that the use of the two-mode method presented in this study can more adequately describe the individual nature of each of the two ECT biases than a single REOF mode examined in previous studies. However, due to the presence of other forms of variability, it is likely that this study's estimate of the ECT bias includes ECT-related bias as well as some aspects of variability that may be associated with sensor changes, intersatellite calibration and/or natural climate variability. The strengths and limitations of the above technique are discussed, as are suggestions for future efforts.

1. Introduction

Satellite-observed outgoing longwave radiation (OLR) datasets have proven to be useful in many climate

studies including analyses on the El Niño–Southern Oscillation (ENSO) (e.g., Gill and Rasmusson 1983; Rasmusson and Wallace 1983; Lau and Chan 1988), the global energy budget (e.g., Gruber and Winston 1978; Gruber and Krueger 1984; Kyle et al. 1985; Harrison et al. 1988; Ramanathan et al. 1989), atmospheric circulation and convection (e.g., Liebmann and Hartmann 1982; Gutzler and Wood 1990; Waliser et al. 1993),

Corresponding author address: Lisanne E. Lucas, Institute for Terrestrial and Planetary Atmospheres, State University of New York at Stony Brook, Stony Brook, NY 11794-5000.
E-mail: slucas@terra.msrc.sunysb.edu

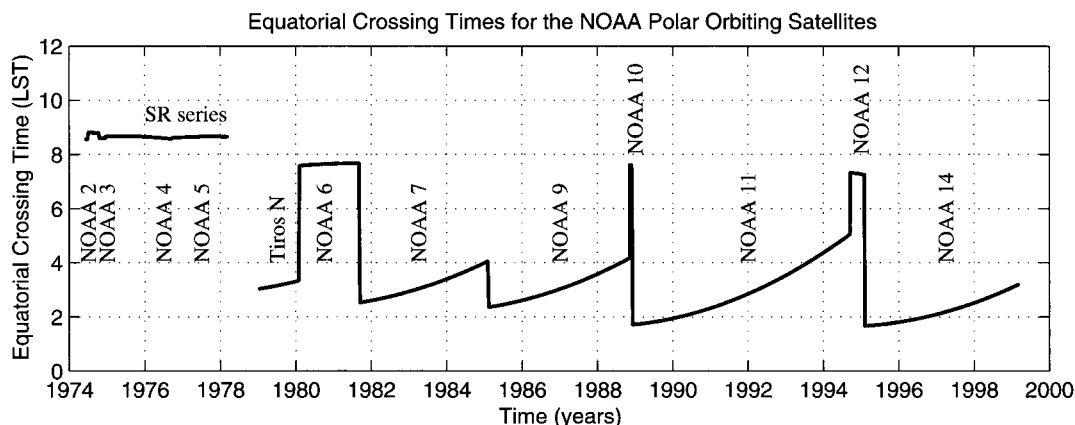


FIG. 1. Equatorial crossing times (ECTs) in terms of local standard time (LST) for satellites used in the construction of the OLR dataset. These ECTs shown are for the morning hours. Note that for each satellite, there is also an afternoon or evening crossing time with the same hour.

intraseasonal variability (e.g., Murakami et al. 1979; Lau and Chan 1988; Hendon and Salby 1994; Jones et al. 1998; Waliser et al. 1999) and precipitation in the Tropics (e.g., Morrissey 1986; Yoo and Carton 1988; Xie and Arkin 1998). These studies, as well as numerous others have been effective in describing the mean global climate as well as many aspects of its variability, particularly shorter-term variability that has timescales of a few years or less.

A number of useful OLR datasets exist to carry out the above sorts of climate studies. These include global data from the Nimbus Earth Radiation Budget (ERB) Experiment (Kyle et al. 1985; Kyle et al. 1993), the Earth Radiation Budget Experiment (ERBE) (Barkstrom 1984), the National Oceanic and Atmospheric Administration (NOAA) operational product (Gruber and Krueger 1984; Gruber et al. 1994), as well as two more recent additions, the Scanner for Radiation Budget (ScaRab) (Kandel et al. 1998) and the Clouds and the Earth's Radiant Energy System mission (CERES) (Wielicki et al. 1996). In addition to the above mission-oriented and operational products there are a number of experimental products, such as those derived from the High-Resolution Infrared Sounder (HIRS) (Ellingson et al. 1989; 1994) and the Television Infrared Observation Satellite (TIROS) Operational Vertical Sounder (TOVS) (e.g., Susskind et al. 1997) on polar-orbiting platforms, as well as others derived from sensors on geostationary satellites (e.g., Minnis and Harrison 1984; Minnis et al. 1991).

Each of the OLR products listed above has its own strengths and weaknesses in regard to accuracy, spatio-temporal sampling, and associated objectives. For example, the ERBE, CERES, and ScaRab missions are particularly attractive for detailed radiation budget studies due to their sampling characteristics (e.g., global, precessing orbits) and/or instrument designs (e.g., broadband). However, these missions are not as useful for studying low-frequency variability due to their rel-

atively short records (i.e., months to a few years) or for examining day-to-day variations in diurnal variability since they are based on polar-orbiting platforms. Geostationary-derived OLR data are very well suited for examining the details of diurnal variability due to their frequent temporal sampling. However, their accuracy is relatively low since the broadband fluxes need to be derived from narrowband radiances, which introduces a number of uncertainties and biases (e.g., Minnis et al. 1991; Gruber et al. 1994). Moreover, each geostationary satellite only samples a particular region of the earth and global coverage is impossible. Given that the operational NOAA OLR dataset is based on (nonprecessing) polar-orbiting platforms and narrowband observations, it is also not well suited for detailed radiation budget studies or examination of the details of the diurnal cycle. On the other hand, it does provide global coverage and a multidecade record. These features make it one of the few sources of satellite data that can be used for studies of low-frequency climate variability, such as variability among ENSO events, decadal variations, or trends. In fact, due to its long record length and continued production (since June 1974), the NOAA OLR dataset tends to be the most widely used of the OLR datasets for diagnostic studies of climate and atmospheric circulation variability.

A drawback of the NOAA OLR record for studying low-frequency variability is that it is composed of data from 12 different satellites, each with its own unique characteristics, such as sensor channels, satellite equatorial crossing time (ECT), and orbital drift rate (Fig. 1). These changes in sampling characteristics can lead to contamination of the natural long-term trends and low-frequency variability in the dataset. Given the potential for signal contamination in the dataset, along with the dataset's extended use by the climate community, it is important to identify, and possibly even correct, any sampling biases in the NOAA OLR dataset to ensure it is as accurate as possible. As Fig. 1 emphasizes, the

ECTs of the satellites that make up the NOAA OLR dataset have changed considerably over the course of the record, implying differences in the manner the diurnal cycle is sampled. Since the diurnal cycle of OLR is generally not symmetric between night and day, the resulting “daily” average obtained from two samples separated by 12 h can become biased relative to the true diurnal average (Vonder Haar and Suomi 1971).

An estimate of the size of the ECT bias in OLR for a 0300/1500 LST satellite ECT can be obtained by comparing time-mean ERBE values of OLR from a “long” overlapping period of the synchronous NOAA-9 and precessing ERBS polar orbiting satellites. Such a comparison shows mean differences ranging between about $\pm 3 \text{ W m}^{-2}$ (see section 4c for more details). The sensitivity of the satellite ECT bias versus ECT was estimated by Waliser and Zhou (1997, Fig. 5; cf., Young et al. 1998) for the Sahara region by comparing two-sample means to the mean of an hourly resolved diurnal cycle estimated by Kondragunta and Gruber (1995) using three ERBE satellites. For the Sahara, the two-sample mean can be biased from the “true” 24-h mean anywhere from about +4 to -8 W m^{-2} depending on the satellite’s ECT. The magnitude of these biases are of a sufficient size to warrant caution in attributing long-term NOAA OLR variations to natural climate variability (e.g., Nitta and Yamada 1989; Morrissey and Graham 1996; Chu and Wang 1997; Waliser and Zhou 1997) and motivates a closer examination of these biases to determine if they can be removed.

A great deal of effort has been expended to try to understand and document the diurnal cycle of OLR. These efforts typically involve the use of diurnally resolving sampling platforms such as geostationary or precessing polar-orbiting (e.g., ERBS) satellites, often in conjunction with models of the diurnal variation of radiation (e.g., Saunders et al. 1983; Duvel and Kandel 1985; Brooks et al. 1984, 1986; Harrison et al. 1988; Hartmann et al. 1991; Rieland and Raschke 1991; Thomas et al. 1995; Hucek et al. 1996; Young et al. 1998). However, little effort has been directed toward describing and correcting the biases in the NOAA OLR dataset in spite of its wide use by the climate community. Adjustments made by Gruber and Krueger (1984) specifically address the biases resulting from changes in instruments and sensor channels (i.e., the narrowband-to-broadband conversion). These corrections were derived from data collected by the NOAA-SR series, *TIROS-N*, NOAA-6, and NOAA-7. They were applied to the entire archived record at the time (1974–84) to render that record as homogenous as possible. Similar adjustments have been incorporated into the narrowband-to-broadband scheme used for the post-1984 data. It should be noted, however, that these adjustments are not likely to fully account for the regional biases that can be introduced into the data due to the diurnal sensitivity of the narrow-to-broadband conversion (e.g., Minnis et al. 1991; Ellingson et al. 1989, 1994). Fur-

thermore, they do not attempt to correct for the changes in the ECT of the satellites used to construct the NOAA OLR dataset.

In regard to the ECT bias in the NOAA OLR dataset, Gadgil et al. (1992) proposed a method that can correct the systematic bias from one satellite (i.e., NOAA-7) to another (i.e., NOAA-SR) by using a simple quadratic relationship. Although this correction is useful for comparing short-term variability, it cannot address the multiple changes in ECT that occur in the current long-term record. A more recent ECT bias correction for the NOAA OLR dataset was explored by Waliser and Zhou (1997). Using a tropical subset (30°N – 30°S) of monthly OLR data they show that transitions between satellites with different ECTs introduce abrupt changes as high as 16 W m^{-2} . Eigen analyses, like the rotated empirical orthogonal function (REOF) analyses performed by Waliser and Zhou (1997), as well as Chelliah and Arkin (1992) before them, are used to isolate artificial spatial loading patterns that are described as “satellite modes.” These modes are known to exhibit a strong loading over land and a weaker loading of the opposite sign over the ocean. They are believed to be an artifact of sampling because the time-dependent amplitudes associated with these modes fluctuate with the changes in the satellite ECTs. Waliser and Zhou used their REOF analysis technique to remove an estimate of the ECT bias from a tropical monthly subset of the OLR dataset.

Based on the encouraging results from the Waliser and Zhou (1997) study, this study was undertaken to explore extensions and refinements of their technique for use on global, daily OLR. In particular, it is designed to focus on, and discriminate between, the two dominant satellite biases associated with changes in ECT—satellite orbital drift and abrupt transitions between afternoon and morning satellites. A central element of this extension is the use of Procrustes targeted REOF analysis (Richman and Easterling 1988) to separately isolate and describe each of these biases in the OLR dataset. The EOF analysis is done in the time domain such that it can extract common patterns of variance in the time series of each grid point (i.e., changes in the satellite ECT). The methods in this study are developed to be more robust and exacting than those of previous studies like Gadgil et al. (1992) and Waliser and Zhou (1997). Further, while earlier studies focused only on tropical subsets of monthly OLR data, this analysis is applied to the entire historical, daily, global OLR dataset. While this particular effort is primarily empirical in nature, parallel efforts are underway (Xie et al. 2000) to try to take advantage of the sampling scheme and diurnal model from ERBE (Brooks et al. 1986). At the conclusion of those efforts, the relative merits of each approach will be assessed to determine which, if either, approach, or a combination, might be feasible for operationally correcting the ECT bias in the NOAA OLR dataset.

In the next section, a detailed description of the dataset and information on the satellites that were used to

TABLE 1. Contributing satellites. A morning satellite is defined as a satellite that has a nominal ECT of approximately “sunrise” and “sunset” (0800 and 2000 LST). An afternoon satellite is defined as a satellite that has a nominal ECT of approximately “midday” and “midnight” (1430 and 0230 LST). Note that the SR series, *NOAA-6*, *-10*, and *-12* are all morning satellites. Grids that are entirely missing are listed within the satellite series.

Name	OLR data start date	OLR data finish date	Nominal ECT (LST)	Number of days	Sensor and window channel
<i>NOAA-3</i>	1 Jun 74	30 Jun 74	0850 morning	30	SR series 10.5–12.5 μm
<i>NOAA-2</i>	1 Jul 74	15 Oct 74	0830 morning	107	
<i>NOAA-3</i>	16 Oct 74	16 Dec 74	0835 morning	62	
<i>NOAA-4</i>	17 Dec 74	14 Sep 76	0840 morning	638	
<i>NOAA-5</i>	15 Sep 76	16 Mar 78	0840 morning	548	
Gap	17 Mar 78	31 Dec 78	—	290	GAP
<i>TIROS-N</i>	1 Jan 79	31 Jan 80	1530 afternoon	396	AVHRR 10.5–11.5 μm
<i>NOAA-6</i>	1 Feb 80	6 Sep 81	0730 morning	584	AVHRR
<i>NOAA-7</i>	7 Sep 81	4 Feb 85	1430 afternoon	1247	AVHRR/2 11.5–12.5 μm
<i>NOAA-9</i>	5 Feb 85	7 Nov 88	1430 afternoon	1372	AVHRR/2
<i>NOAA-10</i>	8 Nov 88	30 Nov 88	0730 morning	23	AVHRR
	1 Jul 90	4 Jul 90		4	
	5 Mar 91			1	
	13 Mar 91			1	
	14 Aug 91			1	
<i>NOAA-11</i>	1 Dec 88	30 Jun 90	1430 afternoon	577	AVHRR/2
	5 Jul 90	4 Mar 91		243	
	6 Mar 91	12 Mar 91		7	
	14 Mar 91	13 Aug 91		153	
	15 Aug 91	14 Oct 92		427	
	16 Oct 92	1 Feb 94		474	
	3 Feb 94	13 Sep 94		223	
<i>NOAA-12</i>	15 Oct 92		0730 morning	1	AVHRR/2
	2 Feb 94			1	
	14 Sep 94	31 Jan 95		140	
	29 Jun 95			1	
	17 May 96	18 May 96		2	
<i>NOAA-14</i>	1 Feb 95	28 Jun 95	1430 afternoon	148	AVHRR/2
	30 Jun 95	16 May 96		322	
	19 May 96	14 Mar 99		1024	
Total Days:				9053	

collect the NOAA OLR is provided. Section 3 presents the methodology used in this study. Section 4 discusses the interpolation of the dataset, and the isolation of the two major ECT biases—satellite drift and abrupt transitions—from the dataset. Section 5 provides a brief summary of the results and discusses the strengths and limitations of this approach. The appendix describes the method for determining the number of statistically significant EOF modes to include in the rotation.

2. Data description

The OLR dataset used for this project is the $2.5^\circ \times 2.5^\circ$ gridded twice-daily satellite dataset produced by the National Centers for Environmental Prediction–National Oceanic and Atmospheric Administration

(NCEP–NOAA). The dataset is 9053 days long, from 1 June 1974 to 14 March 1999. Within this period is a nine-month (290 day) data gap from 17 March to 31 December 1978 due to the failure of the *NOAA-5* satellite (Chelliah and Arkin 1992). There have been several corrections applied to the dataset to account for the changes in instruments and sensor channels, but none that specifically address the changes in the ECT (Gruber and Krueger 1984).

Table 1 shows detailed information about the 12 individual satellites that were used to produce the OLR dataset. There have been many changes to the equipment such as sensors and spectral window channels. The period from 1 June 1974 to 17 March 1978 was collected by the NOAA-SR series (*NOAA-2*–*NOAA-5*). The NOAA-SR series used a scanning radiometer (SR) sen-

sor with a window channel of 10.5–12.5 μm . *TIROS-N*, and its replacements *NOAA-6* and *NOAA-10*, used the advanced very high resolution radiometer (AVHRR) sensor whose window channel is more narrow (10.5–11.5 μm) than the channel on the SR series. The current satellite series, which includes *NOAA-7*, *-9*, *-11*, *-12*, and *-14*, uses the AVHRR/2 sensor with a window channel of 11.5–12.5 μm (Gruber and Krueger 1984; NOAA Polar Orbiter Data User's Guide 1998).

Table 1 also presents the record of the individual satellites and the exact days they contributed to the OLR dataset. Note that the record is dominated by afternoon ECTs (see Fig. 1) and that after 1988, the morning satellites *NOAA-10* and *NOAA-12* were commonly used as replacement satellites to fill in single-day gaps. Table 1 also shows the collection time for the satellite, either morning or afternoon. A morning satellite, for the purpose of this paper, will be defined as a satellite that has a nominal ECT of approximately "sunrise" and "sunset" (e.g., approximately 0800 and 2000). The SR series, *NOAA-6*, *-10*, and *-12* are all examples of morning satellites. An afternoon satellite will be defined as a satellite that has a nominal ECT of approximately "mid-day" and "midnight" (e.g., approximately 1430 and 0230). *TIROS-N*, *NOAA-7*, *-9*, *-11*, and *-14* are afternoon satellites.

Each satellite continuously records information as it orbits the earth from pole to pole, regardless of whether it has a morning or afternoon ECT. The portion of the satellite pass that is collected from the sun side of the earth is designated a daytime pass. The portion on the dark side of the earth is designated a nighttime pass. Each satellite therefore produces a collection of daytime (nighttime) passes for any given day (night) that are mapped to a rectangular grid and used to form a global composite. This twice-daily data is provided from NCEP–NOAA in the form of a daytime series of grids and a nighttime series of grids for each satellite.

In recent years, the addition of a concurrent pair of morning and afternoon satellites has allowed the possibility to use four daily samples in the production of the OLR dataset. Using multiple satellite samples would result in reducing the ECT bias effect although, it would not strictly remove it. NCEP–NOAA has resisted using this approach because the introduction of a four-sample mean could disrupt the long-term homogeneity of the OLR record. Currently, the archived record is predominantly composed of data collected by afternoon satellites, and therefore, the afternoon ECT is the preferred ECT for data collection.

Figure 2 shows a typical 5-day series of the OLR daytime and nighttime grids. These days are taken from 16 May to 20 May 1975 by the *NOAA-4* satellite. They exhibit typical missing data patterns, such as the entire swath missing in Eastern Pacific and Africa for the day 16 May, and the poor coverage of the Arctic region. Figure 3 is a composite of the percent missing data over the record (shown as before and after the nine-month

gap). For the period of 1974–78, the highest values of missing data (45%) occur over the northern most part of North America. This is characteristic of the entire swath persistently missing, a feature that is apparent in Fig. 2. The highest values of missing data ($\sim 45\%$) for the period of 1979–99 come from the regions poleward of 85°N for the daytime series of grids and 85°S for the nighttime series of grids. These missing values are composed of multiple occurrences of gaps that are 60 or more days long.

For this investigation of the ECT biases, we derived the OLR annual cycle solely from the portion of the record sampled by the afternoon satellites. Consistent with NOAA's use of the afternoon ECT as the preferred ECT for data collection, this method establishes the afternoon satellites as the primary ECT for the entire record. Area-weighted daily anomalies used in this study are calculated for the entire dataset with respect to the above-mentioned annual cycle. The area-weighting scheme is based on the square root of a latitudinally dependant sine function [i.e., $\sin(\text{latitude})^{1/2}$] and is applied to each global grid point. Area-weighting of the anomalies in this manner compensates for the extra variance that is introduced by the use of a rectangular global grid where the pole has the same number longitudinal of samples (144; 1 per 2.5° of longitude) as the equator. In order to keep the computational resources of the EOF analysis within practical limits, the daily anomalies are converted to pentad anomalies. This has little effect on the detection of the ECT biases due to the facts that each of the biases are slowly varying and that the shortest series of satellite data (*NOAA-10*) is longer than several pentads. Once the biases are isolated, they will be removed from the daily OLR dataset. In the following sections, unless explicitly noted, OLR will refer to OLR pentad anomalies.

3. Methodology

The goal of this study is to estimate the ECT biases in the daily, global OLR dataset. Our approach involves four principle steps:

- 1) filling the missing OLR grid values by interpolation (see Figs. 2 and 3),
- 2) isolating the ECT drift bias associated with afternoon satellites (see Fig. 1),
- 3) isolating the ECT bias associated with the transitions between morning and afternoon satellites (see Fig. 1), and
- 4) subtracting the estimates of these two ECT biases from the dataset.

a. Filling missing values

Using a modified version of the technique developed by Liebmann and Smith (1996), a series of temporal and spatial interpolations were conducted to fill the

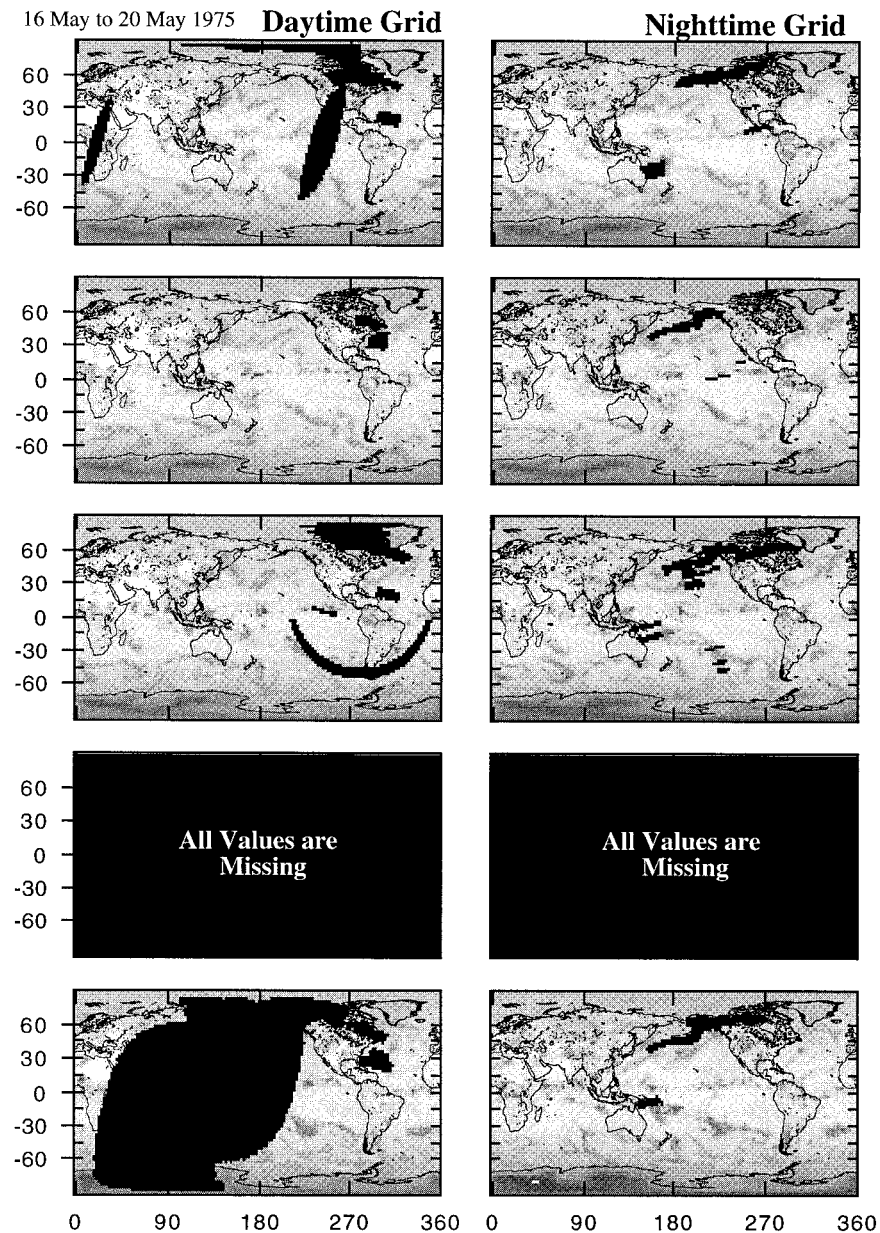


FIG. 2. Typical series of twice daily grids in the OLR dataset. This sequence shows the most common patterns of missing values. These grids are taken from *NOAA-4* on 16–20 May 1975. The daytime (nighttime) ECT is approximately 0830 LST (2030 LST).

missing data in the daily NCEP–NOAA OLR dataset. The 1997 release of the Liebmann and Smith daily OLR dataset would have been used in this study except that it was found to contain an undesirable feature, which was traced to a programming error in one of their gap filling routines. The error caused all temporal gaps longer than three days to be filled with the last known good value. This affected approximately 2% of the entire dataset and caused many grid points to have a constant value. We replaced this filling routine with a linear temporal interpolation that interpolated between the two good points on either side of the gap. This and the

addition of a temporal quality assurance test, were the only modifications made to their technique. The results of the quality assurance test and the gap-filling procedure are presented in section 4. In each of the following steps the daytime series of grids were handled separately from the nighttime series of grids.

The aim of the interpolation scheme is to interpolate over the smallest distance possible in either time or space. This method of interpolation is superior to the traditional spatial-only interpolation used by NCEP because for instances where an entire satellite swath (approximately 1500 km in width) is missing, the error

Percent of Missing Values

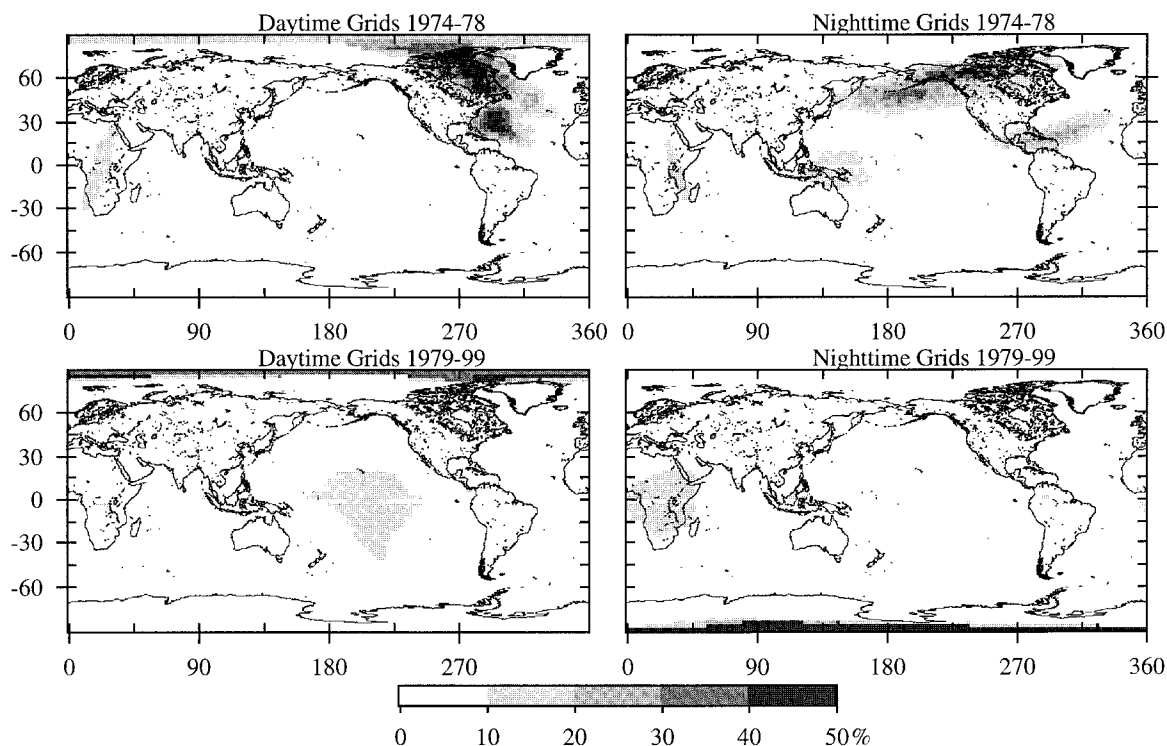


FIG. 3. Percent of data that is missing. The top set of panels are for the period 1974–78 (before the 9-month gap). The bottom set of panels are for the period of 1979–98. Similar to Liebmann and Smith's (1996) Fig. 3.

resulting from interpolating over time at a given point is typically much smaller than the error resulting from interpolating across space at a given time.

The first of five interpolations was made temporally for gaps of one day. The second interpolation was made spatially with the constraint that a value can only be estimated if there are a minimum of three out of the four (above, below, left, and right) "good" values present. This temporal-spatial sequence was repeated once, decreasing the tolerance for the number of "good" spatial data values to a minimum of two. Finally, temporal gaps of less than 60 days were filled by linear interpolation. The remaining missing values—gaps of 60 or more days, and the points at the head and tail of the dataset where temporal interpolation is impossible—are filled by using the value in the other grid (e.g., if the daytime value is missing it will be filled by using the nighttime value). In those places where there are neither a daytime value, nor a nighttime value, spatial interpolation was used after forming a daily average. The position of all interpolated values were marked with a numeric flag that describes the level of confidence in that estimated value.

b. Isolating the afternoon satellite ECT drift bias

The isolation of the actual pattern and the magnitude of the satellite biases was achieved by REOF analysis

of the interpolated OLR dataset. EOF analysis, also called principal components or common factor analysis, is a common technique used to examine the interrelationships between data. This technique decomposes the data into a series of modes, which are composed of an eigenvector (also known as loading; in this case a time series) and an amplitude (in this case a spatial map). The projection of the data onto the eigenvector produces the amplitude of that mode. The unrotated EOF analysis, by definition, acts to maximize for each mode, the variance explained over the entire analysis domain. The first mode returned, therefore, contains the maximum variance that a single mode can account for, and the second mode, contains the highest variance that a single mode can account for and still be orthogonal to the first mode, and so on. This makes the resulting EOF modes very sensitive to domain size and spatial resolution. Rotation of the EOF modes stabilizes the EOF loading and can facilitate their physical interpretation (Richman 1986).

Procrustes target analysis (PTA) is a rotation technique that attempts to linearly transform the EOF loadings into a set of loadings that are as much like a target matrix as possible. This is done by a least-squares fit of the EOF loading matrix to a target matrix, such that $\mathbf{B} = \mathbf{A}\mathbf{T} + \mathbf{E}$; where \mathbf{B} is the target matrix, \mathbf{A} is a matrix of the EOF loadings, \mathbf{T} is the transform matrix, and \mathbf{E}

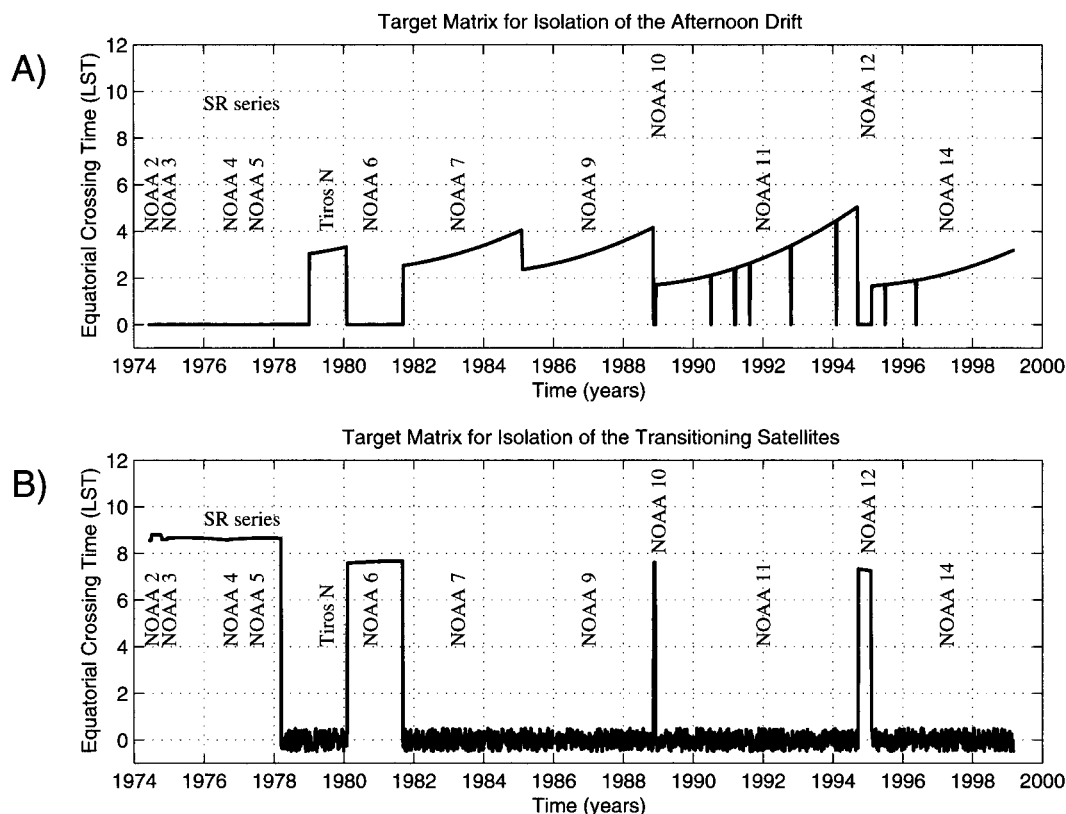


FIG. 4. Target vectors used in rotation of the EOF modes. (a) The target associated with the isolation of the afternoon satellite ECT drift bias. (b) The target used for the transitions between afternoon and morning satellites.

is a matrix of the residuals (Richman and Easterling 1988). Only the statistically significant EOF modes were included in the matrix of the EOF loadings (A). See the appendix for details on determining the statistical significance of EOF modes.

In order to isolate the variability associated with the afternoon satellite ECT drift (see Fig. 1), the approach described above was performed on the data collected by the afternoon satellites. The data collected by the morning satellites was masked out of the dataset by replacing it with zero value anomalies. Therefore, the total variance of the analyzed dataset was composed of only the data collected by the afternoon satellites. Since the rotation target (B) should approximate a model of the ECT drift bias, the exact morning (between 0000 and 1159 LST) ECTs of the afternoon satellites were used. For the periods of time when data were collected by the morning satellites, the ECTs in the target (B) were replaced with zero values. The first vector of the target matrix (B) is shown in Fig. 4a. The other vectors of the target matrix (B) were filled with small amplitude zero-mean random data in order not to influence the rotation.

An indication of a successful rotation would be if one eigenvector strongly resembled the target time series and if the spatial amplitude showed a strong land-sea contrast similar to Chelliah and Arkin's (1992) third

mode or Waliser and Zhou's (1997) fourth mode. That mode would then be selected as the satellite drift-bias mode. Once the satellite drift-bias mode was identified, the satellite-based artificial variance contained within the eigenvector was modeled by a linear regression between the values of the eigenvector and the precisely known ECTs. This relationship was used together with the spatial pattern of amplitudes to construct and remove an estimate of the true ECT drift bias. Note that since the morning satellite data was masked out of this analysis, no correction was applied to that portion of the dataset during this procedure.

c. Isolating the transitioning satellite bias

The drift-bias corrected dataset created in the above step was analyzed for the biases resulting from the transitions between morning and afternoon satellites. A similar REOF procedure to the one that was described in the above section was used to determine the behavior of this portion of the satellite-based artificial variability. In this case, the complete OLR dataset was analyzed (i.e., none of the data was masked out of this procedure).

The target (B) used to represent the transitions between morning and afternoon satellites for the rotation of the EOF modes is presented in Fig. 4b. The portion of the target (B) that is associated with data collected

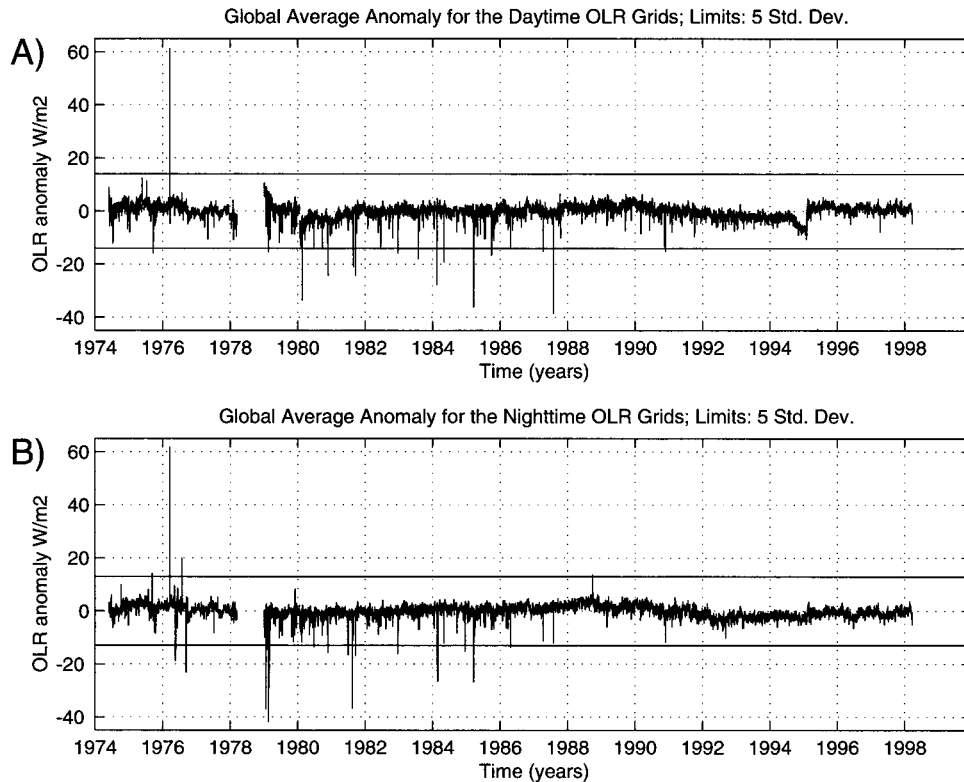


FIG. 5. Global average anomaly for the OLR dataset. The daytime series mean is 216.3 W m^{-2} with a standard deviation of 2.8 W m^{-2} . The nighttime series mean is 212.4 W m^{-2} with a standard deviation of 2.6 W m^{-2} . Twenty-two daytime and 28 nighttime grids were removed from the series that is 9053 days long.

by the morning satellites is represented by the exact ECTs. The portion of the target (**B**) that is associated with data collected by the afternoon satellites consists of a small amplitude, zero-mean random data instead of the exact ECTs. The rationale for using random data is that presumably the bias in the afternoon satellite data was corrected for in the above procedure. Like the previous rotation, the other vectors of the target matrix (**B**) were filled with small amplitude zero-mean random data.

4. Analysis and results

In order to achieve the goal laid out in the previous section, we must first ensure that the data is of good quality and ready for interpolation. The NCEP–NOAA $2.5^\circ \times 2.5^\circ$ gridded twice-daily OLR dataset was first subjected to a pair of quality assurance tests. In each of these steps the daytime series of grids were handled separately from the nighttime series of grids. The first test examined the temporal quality of the data by using the area-weighted global-average anomaly. In this case, the anomaly was formed with respect to the global-average annual cycle. Anomalies that fell within plus or minus five standard deviations from the long-term mean were retained (Fig. 5). The daytime series had

standard deviation of 2.8 W m^{-2} . The nighttime series had standard deviation of 2.6 W m^{-2} . Twenty-two daytime and 28 nighttime grids were flagged as missing ($\sim 0.3\%$ of data) from the series that is 9053 days long.

To test for spatial consistency, each grid point was subjected the spatial “buddy” check used by Liebmann and Smith (1996). The buddy check compares each point to its eight neighboring grid points and marks it missing if it deviates too far from the surrounding points. A total of 35 841 points ($\sim 0.04\%$ of data) were removed from the daytime grids and 38 408 ($\sim 0.04\%$ of data) from the nighttime grids. The majority of the points removed were distributed across the equatorial region.

a. Filling missing values

With the data of suspect quality removed, the process of filling in the missing values by interpolation can proceed. In each of the interpolation steps, the daytime series of grids were handled separately from the nighttime series of grids. The 9-month gap of missing data in 1978 was excluded from the interpolation process and remains as a discontinuity in each of the OLR series. A total of 5.7 million grid points ($\sim 6.2\%$ of data) and

TABLE 2. Statistics associated with the interpolation scheme. The total number of missing points filled for the daytime (nighttime) grids represents 6.2% (6.1%) of the entire dataset.

Interpolation step	Daytime grids		Nighttime grids	
	Number of points filled	Percent of total missing points	Number of points filled	Percent of total missing points
1) 1-day gaps	2 812 676	49.2%	2 818 011	50.0%
2) Spatial—3 of 4 grid points	83 356	1.5	81 343	1.4
3) 1-day gaps	3302	0.1	3 166	0.1
4) Spatial—2 of 4 grid points	236 395	4.1	174 939	3.1
5) Final linear temporal interpolation	2 440 732	42.7	2 266 558	40.2
6) Filled by using the value in the other grid (i.e., day = night)	135 817	2.4	290 898	5.2
7) Spatially interpolated (i.e., points where there are no daytime and no nighttime values)	278	$\ll 0.1$	278	$\ll 0.1$
Total	5 712 556	100.0%	5 635 193	100.0%

5.6 million grid points ($\sim 6.1\%$) were interpolated for the daytime and nighttime, respectively.

During the first step, 2.8 million 1-day gaps in each of the daytime and nighttime series, approximately 50% of the missing data, were filled. This represents the highest percentage of filled values by any step (see Table 2). The second step, which used three or more surrounding spatial points to interpolate the missing grid point, filled approximately 1.5% of the missing values in each of the daytime and nighttime series. The third step, interpolated an additional 0.1% of the data by again interpolating 1-day gaps. The fourth step, which is similar to the second step, used two or more surrounding spatial points to fill 4.1% of the missing daytime points and 3.1% of the missing nighttime points. The final linear temporal interpolation step filled the remaining temporal gaps that are less than 60 days long. This step filled 42.7% of the daytime and 40.2% of the nighttime total missing values. Figure 6 shows those percentages broken down for each gap length. It can be seen that the majority of the data filled in this step is composed of short gap lengths. In fact, 72% (70%) of the daytime (nighttime) points filled in this step are associated with gaps of five days or less. The remaining missing values in each series (2.4%, daytime and 5.2%, nighttime missing values) are filled by using the value in the other grid. A final spatial interpolation is used to resolve the few remaining values ($\ll 0.1\%$) that have neither a daytime value nor nighttime value. All of these values are flagged to show their degree of uncertainty. Some discussion of the influence the above missing values might have on the isolation of the ECT biases is given at the end of section 4c.

b. Isolating the afternoon satellite drift bias

To remove the afternoon satellite drift bias from the OLR dataset we must first determine which REOF mode captures the artificial variability and to what extent that variability is mixed with naturally occurring variability. The analysis of the afternoon satellite drift bias begins

with the examination of each of the EOF modes to determine its relationship to natural variability. While there are 19 statistically significant (see the appendix) modes that account for a total of 29.1% of the anomaly variance, only the first four rotated EOF modes are shown and discussed here.

In general, an EOF analysis decomposes the data into a series of modes, which are composed of an eigenvector (loading or fixed pattern) and an amplitude. These modes are ranked with respect to the variance explained by each such that the first mode returned (and presented) contains the most variance, the second mode contains the second most variance, and so on. In our REOF technique, we are looking to analyze and target the variance in the time domain. This suggests that the EOF analysis be done such that the eigenvectors are time series and the amplitudes are spatial patterns. Procrustes target rotation can then be used to rotate the EOF eigenvectors in a manner that will most fully isolate the biases associated with the changing of the ECT. Due to the nature of the targeted rotation it is not strictly necessary, nor is it expected, that the rotated EOF modes will show uniquely distinguishable climate patterns like those presented in previous REOF studies. Climate patterns, such as ENSO and Madden-Julian oscillation (MJO), would only be uniquely separable if they were orthogonal to the target time series.

Figure 7 shows the first four REOF modes (out of 19) produced by the Procrustes target rotation analysis. These modes are presented in order of decreasing variance. It is readily apparent that the spatial amplitude patterns of modes 1, 2, and 4 do not contain the distinguishable climate patterns similar to those traditionally contained in unrotated EOF spatial patterns. However, the spatial amplitude pattern of the third REOF mode (Fig. 7c) does show a striking resemblance to the “satellite mode” described by Chelliah and Arkin (1992) and Waliser and Zhou (1997).

The third REOF mode (Fig. 7c), which accounts for 1.8% of the anomaly variance, shows a strong land-sea contrast with each landmass well defined by a negative

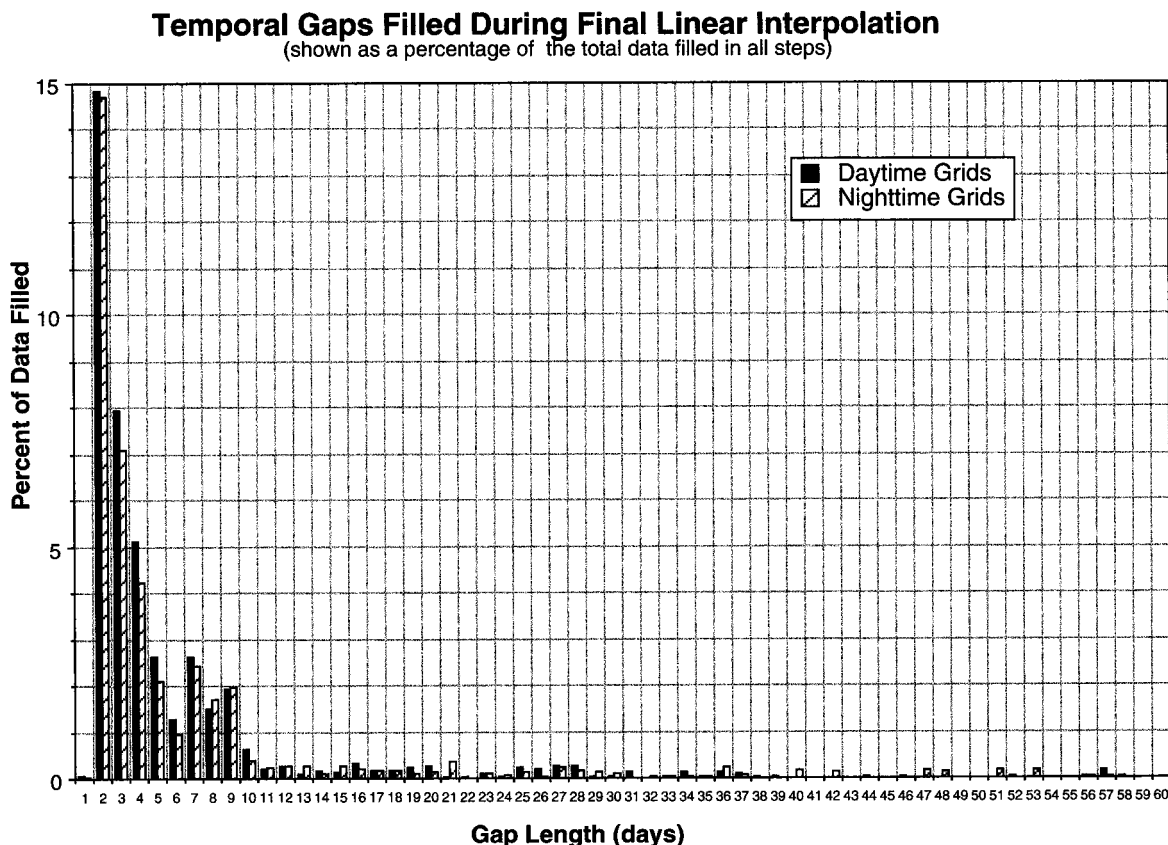


FIG. 6. Temporal gap lengths filled during the final linear temporal interpolation (see item 5, Table 2). The sum of the columns for the daytime (nighttime) grids is 42.7% (40.2%) of the total missing points.

(blue) amplitude. The eigenvector time series has a good correlation ($r = 0.2$; compared to $r < 0.02$ for the other 18 modes; $N = 1808$) with the afternoon satellites ECTs used for the target (**B**; see Fig. 4a). For example, during the period from 1989 to 1995 the eigenvector values have an upward trend from approximately -2 W m^{-2} to $+3 \text{ W m}^{-2}$. This corresponds to the satellite ECT drift in the *NOAA-11* series. Notice that this trend is easily distinguishable from the trend that is associated with ECT drift in the *NOAA-9* series during 1986–89. Using the 5 W m^{-2} range of the *NOAA-11* ECT drift and the spatial amplitude value for the continent of Australia, the OLR difference associated with this satellite drift-bias mode in this region is about 10 W m^{-2} .

To estimate the artificial variability associated with the satellite drift-bias mode, we examined the relationship between the exact afternoon ECTs and the values of the REOF mode three eigenvector. This relationship is the thick black linear regression line shown in Fig. 8. It can be seen from the regression line that there is a positive trend as the ECTs drift toward later afternoon hours. The point at which the regression line crosses zero is approximately 0245 LST suggesting that this is the “common” ECT to which the afternoon satellite data is being calibrated toward. The idea of a “com-

mon” ECT is discussed in a bit more detail in the next subsection.

Figure 9 shows a reconstruction of the satellite drift-bias mode eigenvector using the regression relation in Fig. 8. The synthetic mode explains 0.4% of the anomaly variance in the area-weighted pentad OLR dataset. This “synthetic” eigenvector, weighted by the spatial amplitude, is the part of the anomaly variance that is believed to be due only to the afternoon satellite ECT changes. By using this synthetic eigenvector instead of the actual values of the eigenvector, we hope to retain any natural variability that may be superimposed on the drift-bias in this mode. For example, the peak during 1982–83 in the eigenvector could be associated with the ENSO event of that time. By using the regressed synthetic eigenvector, the part of this mode that actually may contribute to the 1982–83 El Niño will be retained in the data as natural variability. The drift-bias mode was reconstructed using the daily (as opposed to pentad) afternoon satellite ECTs and subtracted from the daily dataset.

c. Isolating the transitioning satellite bias

Now that the ECT biases associated with the afternoon satellites have been removed from the daily OLR

Afternoon Drift Analysis - REOF Modes 1 – 4

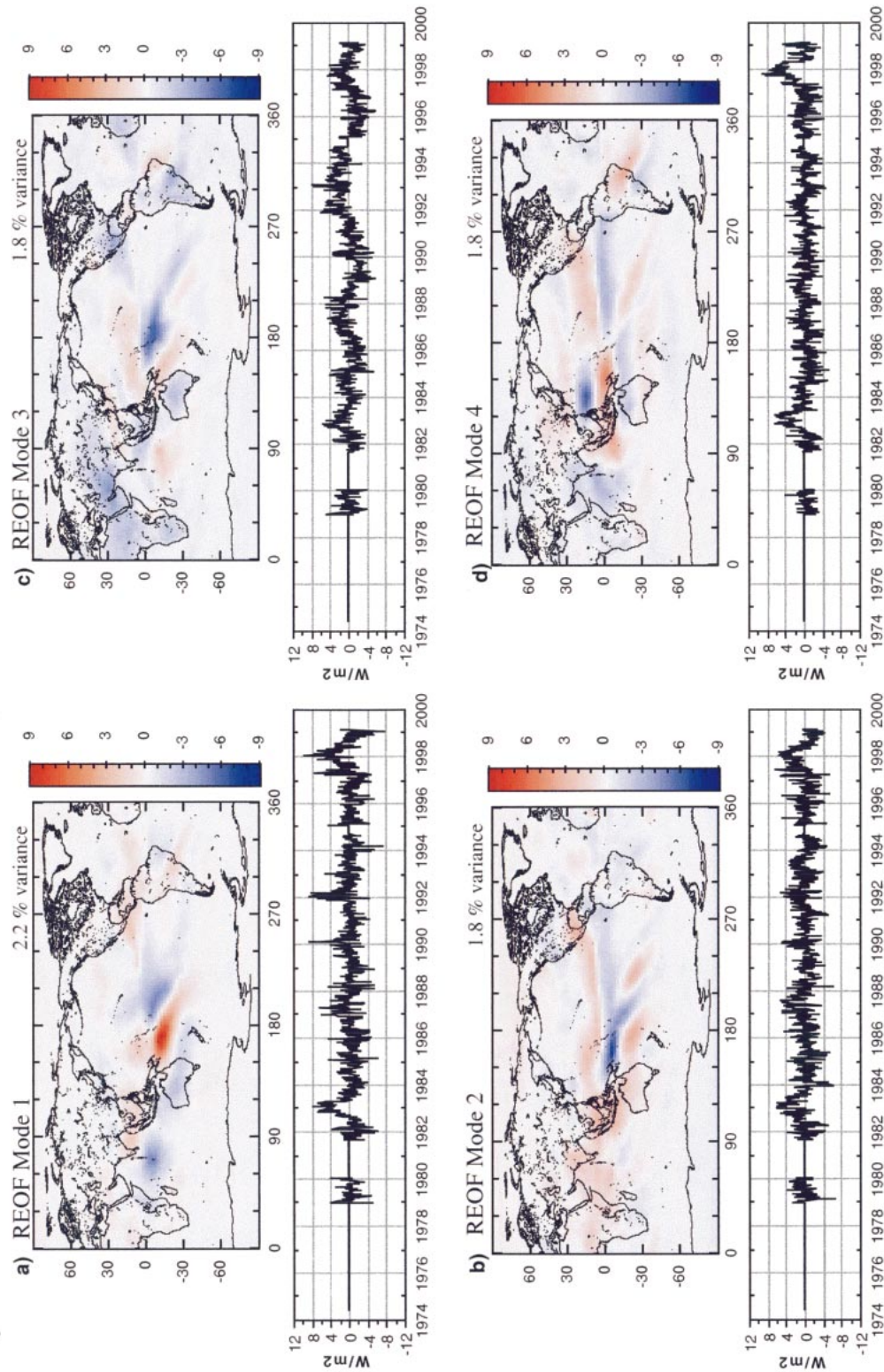


FIG. 7. REOF time series and spatial patterns for the OLR anomalies. The mode associated with the ECT drift bias is mode 3 (C).

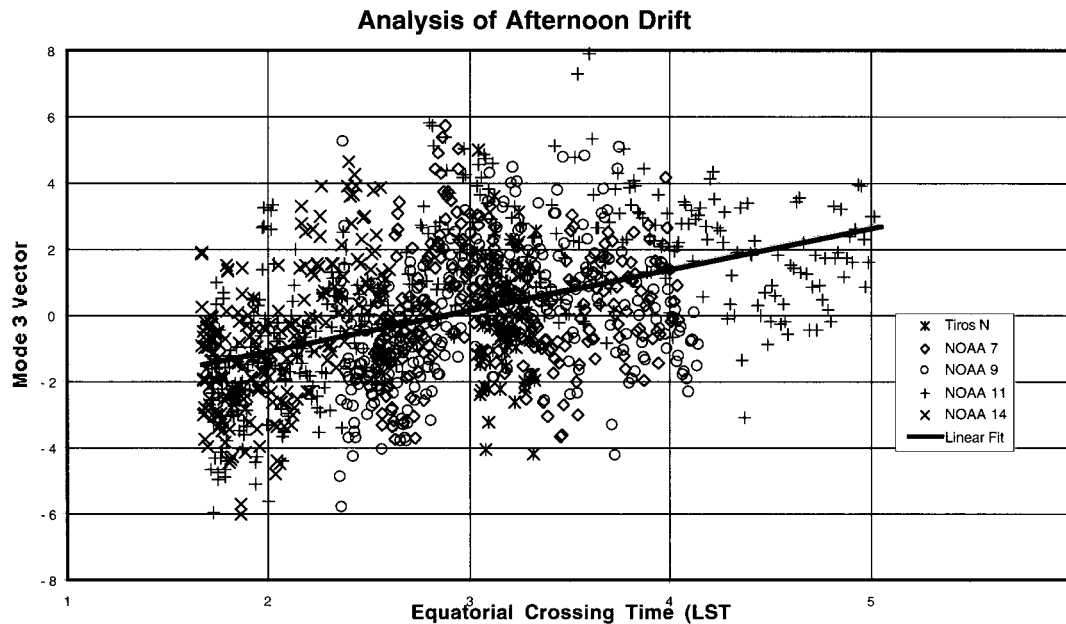


FIG. 8. Scatterplot of the ECT for the afternoon satellite vs the vector values of REOF mode 3 (see Fig. 7c). The thick black line is the best fit linear regression $y = 1.23x - 3.54$. $N = 1313$; correlation = 0.44.

dataset, we can address the issue of the biases caused by the abrupt transitions from morning satellites to afternoon satellites. REOF analysis is performed on the full drift-corrected pentad global OLR anomaly dataset previously described in section 2. The 19 statistically significant EOF modes account for 28.4% of the total anomaly variance.

The first four REOF modes are presented in Fig. 10. Mode 4 (Fig. 10d) has the highest correlation ($r = 0.7$) to the target matrix, which is shown in Fig. 4b. It accounts for 1.7% of the anomaly variance, and shows the characteristic spatial pattern that has been previously described here and in other REOF studies. The eigenvector time series clearly shows the abrupt transition

from the morning satellite *NOAA-6* to the afternoon satellite *NOAA-7* in September of 1981. It also shows the approximately 4 W m^{-2} elevation in the NOAA-SR series from June 1974 to March 1978. Again using the region of Australia as an example, the approximately 4 W m^{-2} loading in the NOAA-SR series, weighted by the spatial amplitude value, gives an OLR bias of approximately -12 W m^{-2} . A negative bias in the OLR values implies that the OLR collected by the morning satellites will be a higher value once corrected, bringing it in agreement with the values collected by the afternoon satellites.

In order to establish the artificial variability associated with the intermittent inclusion of the morning satellites,

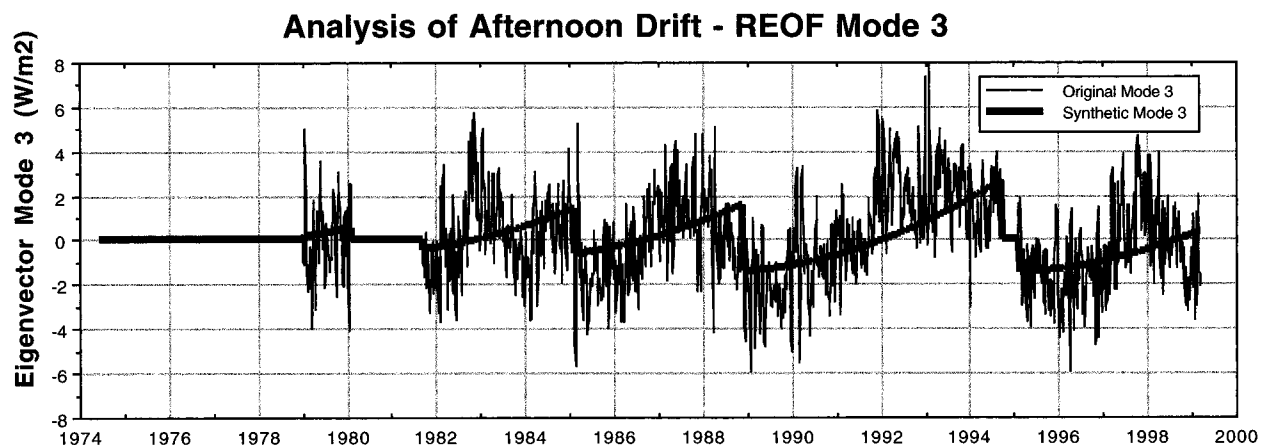


FIG. 9. Estimate of the true ECT drift-bias (thick line) associated with the afternoon satellites. The thick line is based on the regression relation shown in Fig. 8.

Analysis of Satellite Transitions - REOF Modes 1 - 4

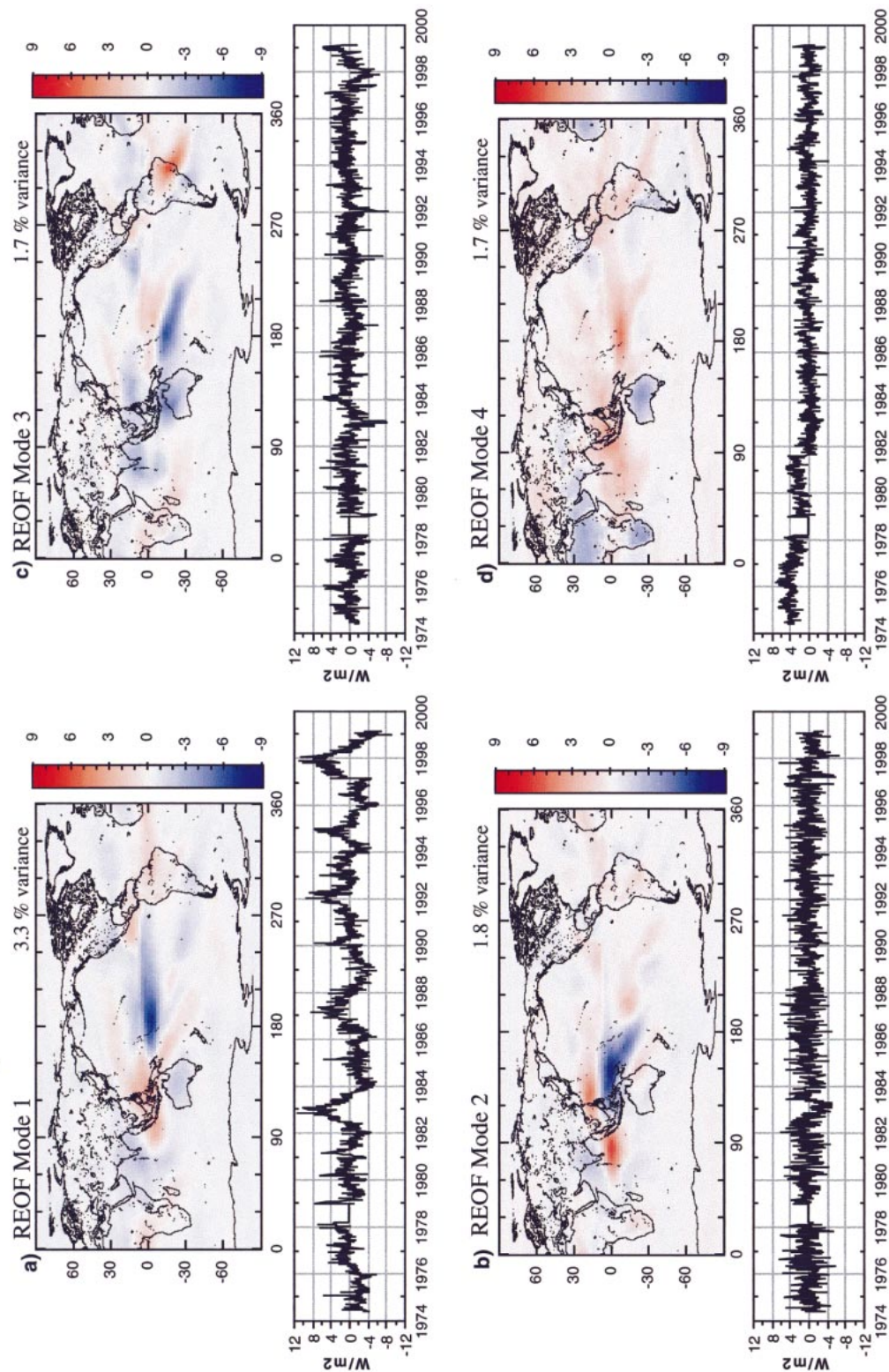


FIG. 10. REOF time series and spatial patterns for the OLR anomalies. Mode 4 is the mode associated with the transitions between afternoon satellites and morning satellites.

Analysis of Satellite Transitions

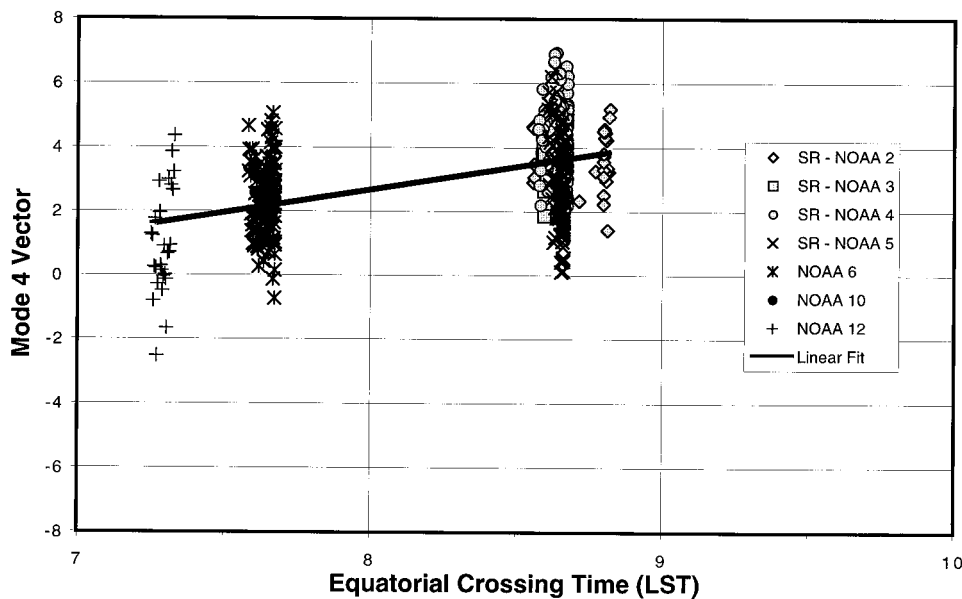


FIG. 11. Scatterplot of the ECT for morning satellites versus the vector values of REOF mode 4 (see Fig. 10d). Thick line is the linear regression $y = 1.42x - 8.65$, $N = 423$; correlation = 0.48.

we must find the relationship between the exact ECTs for morning satellites and the values of the REOF mode 4 eigenvector. This relationship is the linear regression (thick black line) shown in Fig. 11. It can be seen that this has a positive trend as the satellite ECT drifts toward later hours, and a nonzero mean. This supports the notion that the OLR dataset is being calibrated toward a common afternoon ECT. Thus, rather than giving the true diurnal average, the “corrected” form of the dataset would approximate a dataset sampled with an afternoon satellite at a fixed ECT (~ 0245 AM or PM—0245 or 1445 LST). Some notion of how this two-sample approximation of the diurnal mean differs from the true diurnal mean can be obtained by comparing the time-mean OLR obtained from the ERBE sensors (Barkstrom 1984) aboard the precessing ERBS and the NOAA-9 satellites. A comparison for the period February 1985–January 1987 shows that over most of the global oceans the ERBE OLR from NOAA-9 is biased low relative to that from ERBS by about $1\text{--}3 \text{ W m}^{-2}$, while over the nonequatorial regions of Africa, the middle east, Australia, and southern South America, it is biased high by about $1\text{--}3 \text{ W m}^{-2}$.

Figure 12 shows the reconstruction of the satellite transition bias eigenvector. The thick line is the interpolated relationship from Fig. 11. The thin line is the original REOF mode 4 eigenvector (see Fig. 10d). There are positive values for the morning satellites and a zero value for the afternoon satellites. The zero value is consistent with the correction procedure, as presumably the afternoon satellite bias was corrected in the previous

section, and therefore should not require additional correction. This synthetic eigenvector was used, weighted by the spatial amplitude, to construct an estimate of the ECT bias associated with the transitions between morning and afternoon satellites. The component of the satellite bias, which accounted for 0.9% of the anomaly variance, was then subtracted from the dataset.

It should be noted that the introduction of uncertainty in estimating the two bias modes due the filling technique is extremely minor due to the small percentage of data that is missing ($\sim 6\%$) and the location of this missing data. Approximately 60% of the missing data lie outside of the $30^\circ\text{N}\text{--}30^\circ\text{S}$ tropical region and over 70% outside of the $20^\circ\text{N}\text{--}20^\circ\text{S}$ region. Yet about 94% and 81% of the variance associated with either the transition or drift bias modes (i.e., Figs. 7 and 10) lie within the $30^\circ\text{N}\text{--}30^\circ\text{S}$ and $20^\circ\text{N}\text{--}20^\circ\text{S}$ regions, respectively. Thus for the $20^\circ\text{N}\text{--}20^\circ\text{S}$ band, where 81% of the variance in either of the bias/EOF modes is contained, only 30% of the original 6% of the missing data plays a role, or about 2%. In addition, as indicated in Fig. 6, one-day gaps are by far the most predominate gap length and there is little uncertainty in filling such a short gap length. An indirect illustration of the insensitivity of the bias mode(s) to small amounts of what might be considered “noise” is given in the appendix, namely associated with the discussion of Fig. A3. This figure shows that the bias mode extracted via EOF rotation is very stable to the inclusion or omission of higher-order modes. Finally, considering that about 70% of the gap lengths are less than 10 days and the fact that the bias

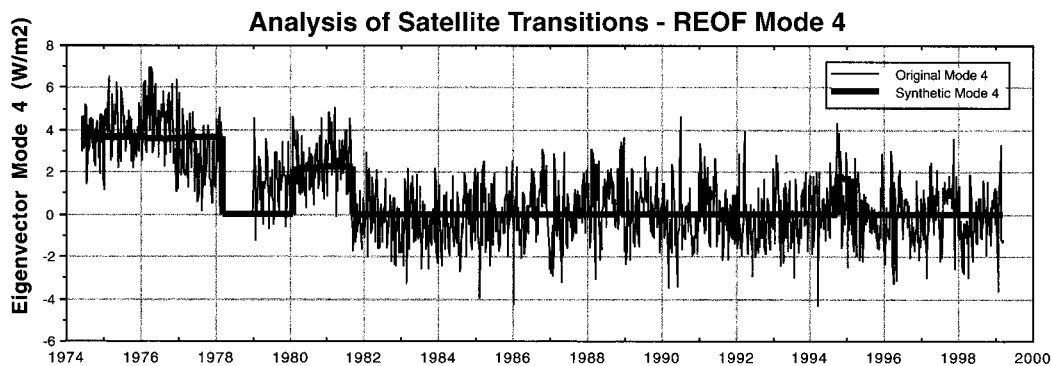


FIG. 12. Estimate of the artificial variability (thick line) captured in the fourth REOF. This variability is associated with the ECT change due to the transition between afternoon satellites and morning satellites. The thick line is based on the regression shown in Fig. 11. The thin line is the actual eigenvector time series from the fourth REOF mode (see Fig. 10d).

modes are very low-frequency modes, in conjunction with the rest of the discussion above, indicates the trivial influence the method of data filling has on the estimate of the biases.

5. Summary and discussion

The goal of this study was to derive a method for estimating the ECT biases in the daily, global NOAA OLR operational dataset. The methods shown here were developed to be more exacting than those of previous studies like Gadgil et al. (1992) and Waliser and Zhou (1997). The dataset used for this project was the 2.5° -gridded, twice-daily OLR dataset produced by NCEP–NOAA with all missing values filled by interpolation. The interpolation consisted of using a modified version of the temporal–spatial interpolation method introduced by Liebmann and Smith (1996). Approximately 6% of the twice-daily OLR data were interpolated before forming the daily averages. These daily averages were used to make the pentad anomalies for the rotated EOF (REOF) analysis. Procrustes targeted EOF rotation analysis was performed on the global OLR dataset to isolate the two major ECT biases—afternoon satellite orbital drift and abrupt transitions between morning and afternoon satellites. Results from the analysis show that changes in ECTs can cause large regional biases over both land and ocean (e.g., Vonder Haar and Suomi 1971).

The afternoon satellite ECT drift bias is isolated by the third targeted REOF mode of the afternoon satellite only dataset (see section 2 for details) and accounts for 0.4% of the pentad anomaly (about the annual cycle) variance. The spatial amplitude (Fig. 7c) shows sharp land–sea contrasts, which is consistent with the REOF modes found in earlier ECT bias studies. The eigenvector time series captures a slowly varying trend that appears to be directly related to the orbital drift of afternoon satellites. For example, during the period of

December 1988–September 1994, the eigenvector time series increases as the *NOAA-11* satellite drifts from a 0145 LST crossing time to a 0500 LST crossing time. This ECT drift introduced a time-dependent bias of approximately 10.5 W m^{-2} in the OLR values over most tropical landmasses.

A second targeted REOF analysis was then performed on the ECT drift-corrected pentad OLR anomaly dataset (i.e., the dataset after the above estimate of the drift mode was subtracted; see section 2) to isolate the ECT bias associated with the transitions between afternoon satellites and morning satellites. The transition bias was captured by the fourth targeted REOF mode, which accounted for 0.9% of the pentad anomaly variance. Like the drift-bias mode, the spatial amplitude (Fig. 10d) shows distinct land–sea contrasts in the tropical regions. Taken together with the eigenvector time series, this transition-bias mode shows that the OLR values over tropical landmasses for the NOAA-SR satellite series are biased by approximately 12 W m^{-2} lower than those collected by the afternoon satellites.

For each component of the bias estimate (i.e., drift and transition), a synthetic version of the eigenmode, rather than the exact values, was used to remove the bias-driven variability from the OLR dataset. This was done to try to ensure that only the variability associated with the ECT biases is removed. The synthetic eigenmodes were made up of the spatial amplitude pattern of the satellite bias mode and a synthetic eigenvector time series. The synthetic eigenvector time series was formed from the linear regression between the actual values of the bias-mode eigenvector and the exact ECTs for the satellites. This allows the natural variability, which may have a nonzero projection onto the satellite bias mode, to remain in the OLR dataset after the satellite bias is subtracted. It should be noted that each day of the OLR dataset is corrected for only one type of bias. The afternoon drift-bias mode is used to correct the portion of the data collected by afternoon satellites,

and the transition-bias mode is used to correct the data collected by the morning satellites.

To test the sensitivity of our bias estimate to the linear assumption used in the above-mentioned regression (i.e., Fig. 8 and 11), we compared the biases to those obtained when a second-order regression was used for each bias (transition and drift). For each regression case, the three-dimensional bias structure (time, latitude, longitude) was produced by adding the transition and drift biases together. We computed the correlation and root-mean-square (rms) difference between the two bias estimates. The globally averaged rms and correlation values between the two bias estimates were 0.19 W m^2 and 0.97, respectively. The rms outside the Tropics was exceptionally small (~ 0). This resulted in lower correlations in the extratropics because the correlation was essentially between noise. If only the 30°N – 30°S region was considered, then the rms was about 0.33 W m^{-2} and the correlation was about 0.98. Thus, the bias estimate is fairly insensitive to the linear assumption used to derive the relation between ECTs and bias-mode eigenvector values.

The improvements associated with this ECT bias-estimation procedure, over previous methods, are contained in the separation of the two major ECT biases—satellite orbital drift and abrupt transitions between afternoon and morning satellites—and the use of the Procrustes targeted REOF analysis technique. Applied together, these techniques provided a way to attempt to establish a “common ECT” to which the dataset would be corrected toward (i.e., the afternoon ECT; 1445 LST). Further, it allows for the potential application of this procedure to any future OLR data, provided that is collected by satellites with ECT similar to those analyzed in this study.

The two REOF bias modes produced in this study are nearly orthogonal to each other, having less than 3% of their variance in common ($r = 0.17$). This near orthogonality between them suggests that the use of this two-mode method can more adequately depict the individual nature of each of the two ECT biases than a single REOF mode. By comparing the reconstructed biases (the dot product of the eigenvector and the amplitude) produced from the single satellite mode in the Waliser and Zhou (1997) study (see their Fig. 3d) to the pair of modes found here (Figs. 7c and 10d) we can make a quantitative assessment of their shared characteristics. We find that the Waliser and Zhou bias shares approximately 17% of the variance in the bias mode that was found in this study (for the tropical region of 30°N – 30°S). The afternoon-drift mode can account for approximately 10% of this shared variance with the satellite transition-bias mode accounting for the remainder.

To help understand some of the limitations of the above technique as well as the inherent difficulties associated with the ECT bias problem, Fig. 13 shows a tropically averaged (30°N – 30°S) subset of the monthly OLR anom-

alies for the original NCEP–NOAA dataset (black line), the ECT bias-corrected OLR dataset produced in this study (dashed line), and the ECT bias-corrected OLR dataset produced in the Waliser and Zhou (1997) study (gray line). While some of the variation depicted by these curves is expected to result from natural variability, there are several periods that display what is likely to be artificial variability, especially when one considers the satellite transitions/drifts displayed at the bottom of the figure. The sources of this artificial variability could arise from aspects of the ECT bias that were not removed, sensor changes, narrowband-to-broadband model/diurnal dependencies (e.g., Minnis et al. 1991; Ellingson et al. 1989; 1994), and possibly sensor/calibration drift. In discussing these sources of artificial variability, and the periods of the record they might be influencing, it is useful to consider the morning satellite (e.g., SR, NOAA-6, -10, -12) and afternoon satellite periods (e.g., TIROS-N, NOAA-7, -9, -11, -14) separately.

With respect to the variations in the tropical average OLR for the morning satellites, there are fairly sharp transitions occurring between morning and afternoon satellites (e.g., before and after NOAA-6, after NOAA-12). On one hand, this raises a question as to how well the ECT transition bias has been estimated, especially as it relates to the tropical average. On the other hand, these transitions appear to demonstrate that the OLR record likely contains some sensor and/or intersatellite calibration biases as well. For example, the sampling time periods of all the morning satellites are within about 1 h of each other (Table 1, Figure 1). This suggests that the representation of the tropical mean OLR from these morning satellites should have similar ECT biases relative to that sampled by the afternoon satellites, at least with respect to their sign. However, the data from the SR series is biased high relative to the mean, while that from the morning NOAA series is biased low relative to the mean. This difference cannot be attributed to ECT based on the similarity of the sampling times but is likely to be attributed to the sensor change and/or intersatellite calibration, which could include narrowband-to-broadband model dependencies (Gruber and Kruger 1984; Gruber et al. 1994). Adding to the difficulty of identifying the source(s) of these variations is the climate change/shift that occurred in tropical SSTs and convection around the late 1970s (e.g., Trenberth 1990; Graham 1994; Morrissey and Graham 1996). For our estimate of the ECT transition bias, the rotation target (see Fig. 4b) was constructed with the assumption that the nature of the bias would present itself in a common manner (e.g., similar in amplitude and sign) for crossing times that are similar to each other. However, due to the presence of these other forms of variability associated with the morning satellites and their periods of operation, it is likely that our estimate of the transition bias includes ECT-related bias as well as some aspects of variability that may be associated with sensor

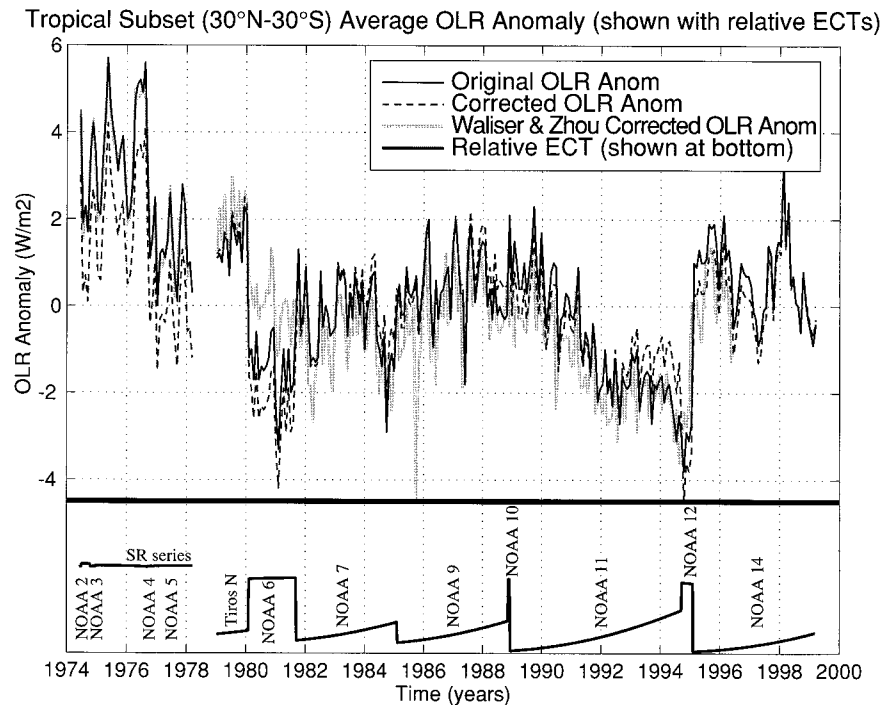


FIG. 13. Tropical-subset monthly averaged OLR anomalies produced in this study shown with the Waliser and Zhou (1997) monthly tropical OLR anomalies for comparison. The satellite ECTs are shown at the bottom for reference only. For the exact crossing times see Fig. 1.

changes, intersatellite calibration and/or natural climate variability.

With respect to the variations in the tropical average OLR (i.e., Fig. 13) for the afternoon satellites, one feature that stands out is the decreasing trend during the early 1990s. This feature appears to occur in conjunction with the ECT drift of *NOAA-11* and again raises a question of how well the ECT drift bias has been estimated, especially in terms of its influence on the tropical average. Note this downward trend is not likely to be related to the lengthy but modest El Niño that occurred during this period (Trenberth and Hoar 1996) since the tropical average OLR typically increases during an El Niño (e.g., Chou 1994; Zhang et al. 1996). As with the transition bias, there are inconsistencies in the manner the drift appears to be projecting itself onto the tropical mean. For example, the drifts associated with *NOAA-7*, *-9*, and *-14* do not appear to exhibit the same type of downward trend. Similar inconsistencies are seen in the global averages shown in Fig. 5. This raises the question of what might be responsible for such a dramatic trend in the tropical average during this period. One possibility might be related to the fact that the afternoon sampling time associated with *NOAA-11* drifts later into the afternoon (by about an hour) than the sampling time for the other three afternoon satellites. Given that there is only this one satellite and period to base our estimate of the ECT drift bias for this sampling time upon (i.e.,

slope in Fig. 8), we may be underestimating the bias versus drift relationship, especially if this period is also being influenced by natural variability (e.g., El Niño). Further, if there are nonlinear effects in the way the drift bias influences the data this aspect would not be well captured by our linear techniques (i.e., EOFs in conjunction with Figs. 8 and 11). Some evidence for such a nonlinearity, at least at one tropical location, is given by the estimate of the diurnal cycle over the Sahara and its polar orbiting sampling bias presented in Waliser and Zhou (1997; their Fig. 5).

An additional possibility for the downward trend during the 1990s is a sensor/calibration drift. Along with the lack of a similarly observed feature during the *NOAA-7* and *-9* periods, additional evidence for this possibility is given by the time series of OLR anomalies averaged over high latitudes (e.g., 45° – 80° ; not shown). These plots show evidence of a downward trend over both high-latitude regions during the period associated with the *NOAA-11* but not *NOAA-7* or *NOAA-9*. Note that the ECT bias should be greatly reduced over high-latitude regions due to overlapping coverage of subsequent passes, and especially over the southern latitudes due to the prevalence of ocean versus land (e.g., Figs. 7c, 10d; Harrison et al. 1988). Even with such leading information, the likelihood of a sensor/calibration-related bias is still mostly a matter of speculation as there is very little tangible information by which to assess

this as a possible source of bias. As with the morning satellites, there is also some evidence of a bias related to a sensor change in the afternoon satellites that influences the tropical average. Specifically, the sampling time of *TIROS-N* is similar to the initial sampling times of all the other NOAA-series afternoon satellites. However, its tropical average is biased high relative to these other satellites/periods. To determine if this difference was associated with natural variability or a sensor change, it might be possible to analyze other datasets that are not affected by the same ECT sampling bias.

While the original intention was to produce a ECT bias correction that was considered robust enough to implement operationally, the remaining uncertainties regarding the method and associated dataset described above suggest that further refinements be made before proceeding to that stage. Moreover, based on the analysis undertaken in this study, it is suggested that future efforts to estimate the ECT bias in the NOAA OLR dataset employ either radiation models that specify observed cloud amounts (e.g., Zhang et al. 1995) or utilize the ERBE diurnal cycle model (Brooks et al. 1986) or similar constructs (e.g., Young et al. 1998). The former was explored in the early stages of this project but the model OLR fields analyzed did not match the observed fields sufficiently well at the time to continue with that avenue of analysis. Presently, the latter alternative appears to hold promise and is currently under exploration (Xie et al. 2000). Until further progress is made regarding the diagnosis and understanding of the artificial components of the variability in the NOAA OLR dataset, we recommend that considerable caution be exercised when trying to apply this dataset to studies of low-frequency climate variability, and in particular to questions concerning anthropogenic climate change.

Acknowledgments. This project was supported by funding from the NOAA–NASA Climate Change Enhanced Data Set Program, Grant NA76GP0450. The foundation of this study stems from the first author's Masters thesis at the State University of New York, Stony Brook. In this regard, the first two authors would like to thank Professors Robert Wilson and Minghua Zhang for their comments and suggestions regarding this work. We also thank Michael Richman for his help and advice on using the Procrustes targeted rotation technique. This study's analysis and presentation benefited from the use of the Seaspace Corporation's TeraScan software system.

APPENDIX

Determination of Statistically Significant Modes to Rotate

In order to determine which EOF modes to use in the rotation, we used a modified form of the Preisendorfer *N*-rule significance test (Preisendorfer et al. 1981). An

example of the previous use of the *N*-rule test on EOFs can be found in Waliser and Zhou (1997). In the *N*-rule test, a series of EOF analyses are performed on random-number datasets that have the same dimensions in time (*N* points) and space (*P* points) as the analyzed OLR dataset. The results of those random-data EOF analyses are grouped together according to mode number and sorted to find the highest eigenvalue percentages (i.e., the percent of total anomaly variance described by the eigenvalue) for each mode number. When this procedure is performed on 100 different random datasets, the highest eigenvalue percentage for each mode denotes a 99% significance level, the second highest eigenvalue percentage for each mode denotes a 98% significance level, and so on. The idea being that if a mode returned from the EOF analysis of OLR data has a percentage that exceeds the highest percentage for that mode in the analysis of the 100 random-number datasets, then it can be called significantly different, at the 99% confidence level, from random noise. In this study, an *F* test (Hoel 1984) was added to the *N*-rule significance test to find the minimum number of significant modes to include in the rotation. This is done by comparing the ratio of the variance explained by rotating all of the significant modes to the variance explained by rotating some number less than all of the significant modes until that ratio is no longer statistically significant.

The above procedure was performed for the area-weighted pentad OLR anomaly dataset. However, to make an assessment that was as conservative as possible, we attempted to estimate the number of independent samples in the OLR dataset with respect to time and space (*N* and *P*, respectively). The number of pentads (*N*) in the OLR dataset is 1735 and the number of spatial points (*P*) equals 10 512 (73×144 grid points). The autocorrelation computed in the zonal direction (constant latitude), averaged over time and longitude, suggested a decorrelation scale ($1/e$) as large as 16° (~ 6.5 points). Similarly, the autocorrelation computed in the meridional direction (constant longitude) at each zonal point, averaged over time and latitude, suggests a decorrelation scale as large as 7.5° (~ 3 points). Together, these two factors reduce *P* from 10 512 to 506 (23×22). The autocorrelation computed in the temporal direction at each spatial point, averaged over the meridional direction, suggests that the decorrelation scale is just under two pentads. This reduces the effective number of independent samples in time to $N = 964$.

Based on the above *N* and *P* values for the OLR dataset, the *N*-rule significance test was performed using 50 "random-number" datasets. The random-number datasets were generated by selecting data points from the pentad OLR anomaly dataset and shuffling, with respect to time and space, before each EOF analysis. This allowed us to create a "random-number" dataset that was more representative of the characteristics of our data than a true random-number dataset would. Figure A1 shows the results of the *N*-rule test. The solid thick line

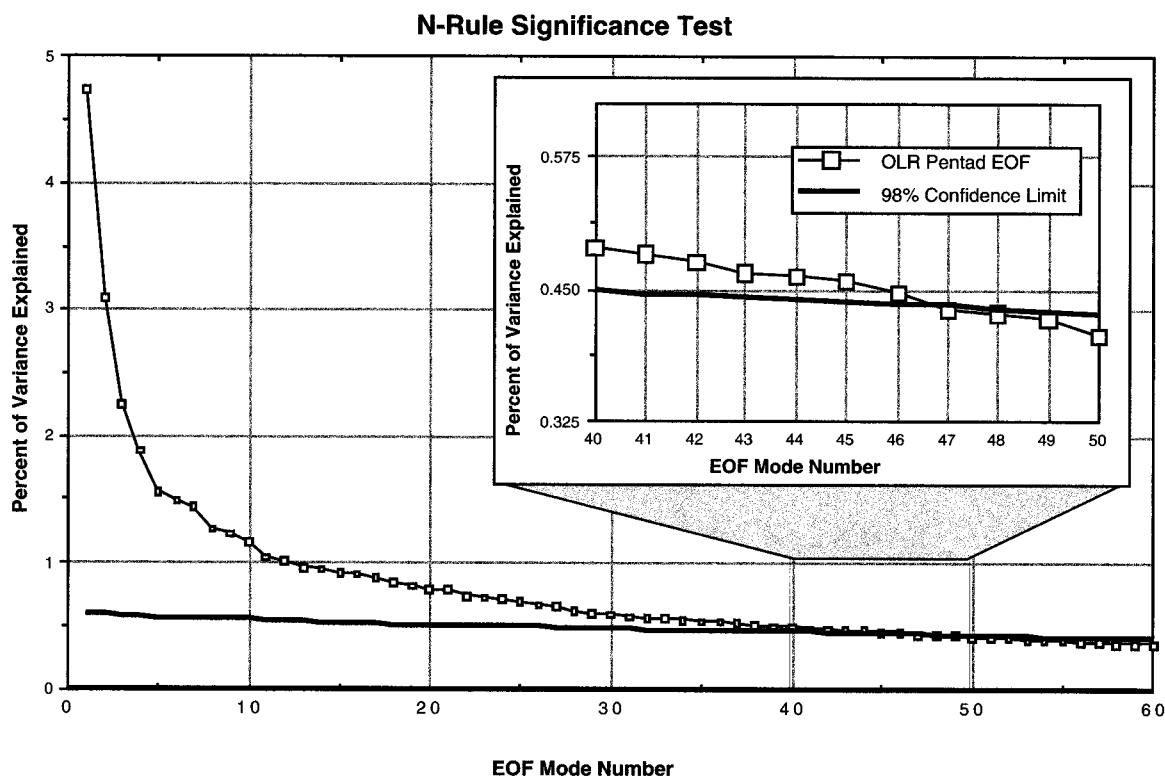


FIG. A1. Eigenvalues, in terms of percent of anomaly variance explained, for the pentad OLR dataset. The thick line indicates the 98% confidence level as determined by the Preisendorfer *N*-rule test.

in the plot shows the 98% confidence limits. The thin line with squares shows the eigenvalue percentages from the OLR EOF decomposition. For the OLR dataset, the first 46 modes are judged to be significantly different from random noise at the 98% confidence limit and thus were the modes considered for inclusion in the *F*-test procedure. The total amount of pentad anomaly variance explained by the first 46 modes was 44%.

The *F* test is useful in testing the equality of two variances, which is a way to test that the two samples have been drawn from the same parent population. It has previously been established, by the *N*-rule test, that the first 46 EOF modes are significantly different from randomized data. Using the variance explained by this number of modes (46), we compared the variance explained by a lesser number of modes ($46 - n$), varying n until the ratio exceeded the critical *F* value. Above this critical value of n , the two samples can no longer be established as being drawn from the same parent population at a 95% confidence level. To make a liberal estimate of the number of modes to include in the rotation, we selected two more than the critical number. The *F* ratios are shown in Fig. A2. The thin line represents the critical *F* values for the 95% significance level. The line with squares is the ratio of the variance explained by 46 modes to the variance explained by (46

$- n$) modes. It can be seen that 17 is the number of modes at which the *F* ratio exceeds the critical *F* value, therefore, 19 ($2 + 17$) is the minimum number of modes included in the rotation without degrading the variance of the retained data and thus, presumably, the ECT bias signal. The first 19 EOF modes account for 28% of the anomaly variance.

To validate the *F*-test approach described above, we performed a “rotation sensitivity” test on the results from an EOF analysis of a pentad OLR anomaly dataset. The sensitivity test was devised to determine how the integrity of the ECT bias mode changed by rotating a lesser number of modes ($46 - n$) compared to rotating all 46 significant modes. This sensitivity test examined the correlation between the satellite bias mode found in each of the ($46 - n$) rotations to the satellite bias mode found using the full 46 modes. Figure A3 shows the results of this sensitivity test. It can be seen that the correlation remains fairly constant for rotations for 25–45 modes. This suggests that although the additional variance contained in the higher number modes is significantly different from randomized data, it is not related to the ECT bias. The correlation for the rotation of 19 modes is 0.95 indicating that the integrity of the ECT bias is only minimally enhanced by the inclusion of the addition variance.

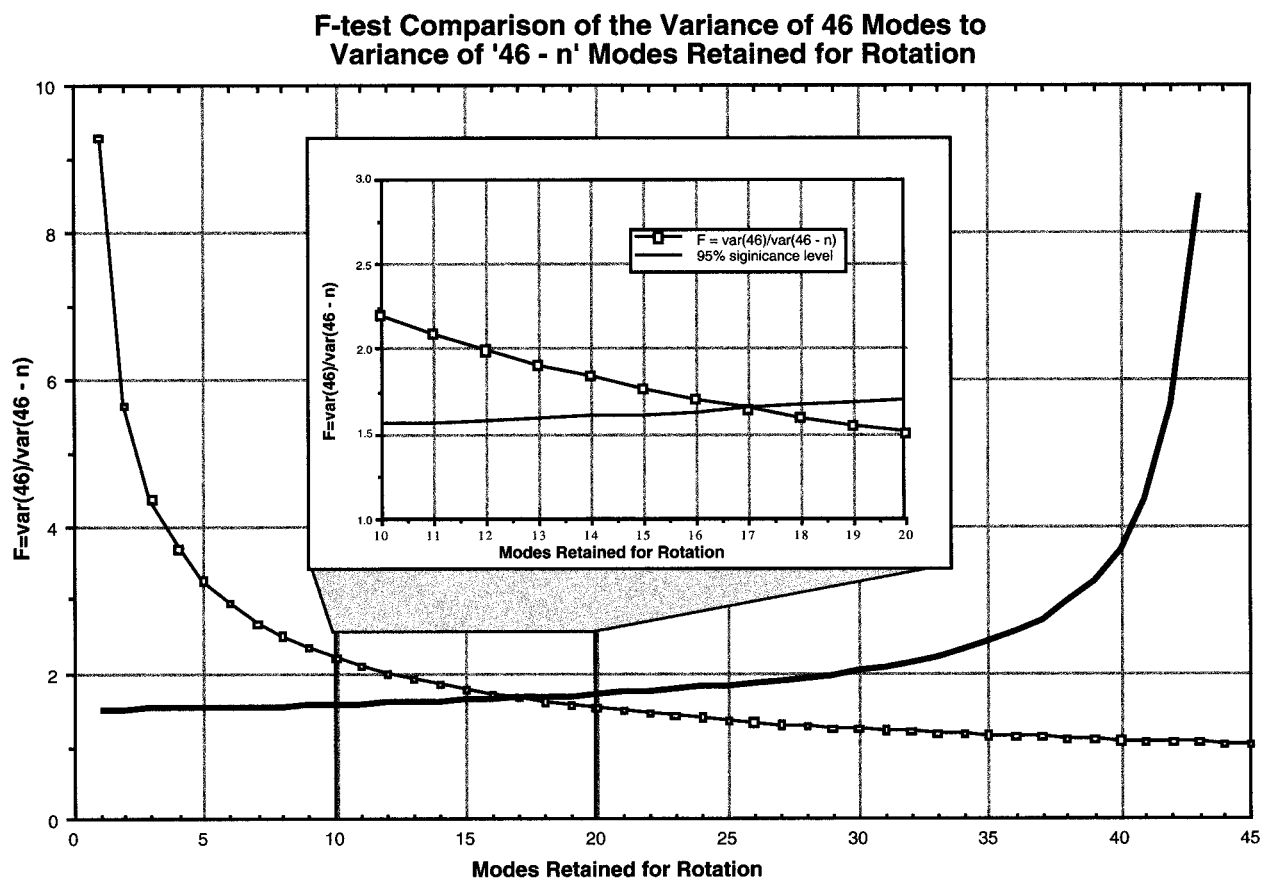


FIG. A2. Results from the F test used to find the minimum number of significant modes to include in the rotation. The thick line represents the 95% significance level.

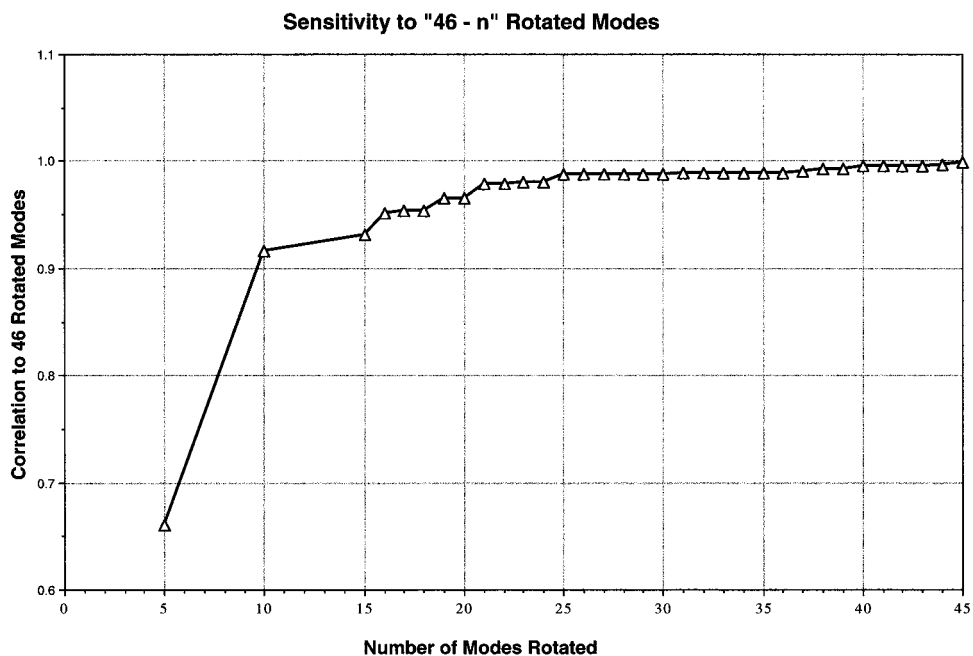


FIG. A3. Sensitivity test to confirm that the ECT bias is adequately described by the rotation of 19 EOF modes.

REFERENCES

- Brooks, D. R., and P. Minnis, 1984: Comparison of longwave diurnal models applied to simulations of the Earth Radiation Budget Experiment. *J. Climate Appl. Meteor.*, **23**, 155–160.
- , E. F. Harrison, P. Minnis, J. T. Suttles, and R. S. Kandel, 1986: Development of algorithms for understanding the temporal and spatial variability of the Earth's radiation balance. *Rev. Geophys.*, **24**, 422–438.
- Barkstrom, B. R., 1984: The Earth Radiation Budget Experiment (ERBE). *Bull. Amer. Meteor. Soc.*, **65**, 1170–1185.
- Chelliah, M., and P. Arkin, 1992: Large-scale interannual variability of monthly outgoing longwave radiation anomalies over the global Tropics. *J. Climate*, **5**, 371–389.
- Chou, M. D., 1994: Coolness in the Tropical Pacific during an El Niño Episode. *J. Climate*, **7**, 1684–1692.
- Chu, P.-S., and J.-B. Wang, 1997: Recent climate change in the tropical western Pacific and Indian Ocean regions as detected by outgoing longwave radiation records. *J. Climate*, **10**, 636–646.
- Duvel, J. F., and R. S. Kandel, 1985: Regional-scale diurnal variations of outgoing infrared radiation observed by METEOSAT. *J. Appl. Meteor.*, **24**, 335–349.
- Ellingson, R. G., D. J. Yanuk, H.-T. Lee, and A. Gruber, 1989: A technique for estimating outgoing longwave radiation from HIRS radiance observations. *J. Atmos. Oceanic Technol.*, **6**, 706–711.
- , H.-T. Lee, D. Yanuk, and A. Gruber, 1994: Validation of a technique for estimating outgoing longwave radiation from HIRS radiance observations. *J. Atmos. Oceanic Technol.*, **11**, 357–365.
- Gadgil, S., A. Guruprasad, and J. Srinivasan, 1992: Systematic bias in the NOAA outgoing longwave radiation dataset? *J. Climate*, **5**, 867–875.
- Gill, A. E., and E. M. Rasmusson, 1983: The 1982–83 climate anomaly in the equatorial Pacific. *Nature*, **305**, 229–234.
- Graham, N. E., 1994: Decadal-scale climate variability in the tropical and north Pacific during the 1970s and 1980s—Observations and model results. *Climate Dyn.*, **10**, 135–162.
- Gruber, A., and A. Krueger, 1984: The status of the NOAA outgoing longwave radiation dataset. *Bull. Amer. Meteor. Soc.*, **65**, 958–962.
- , R. Ellingson, P. Ardanuy, M. Weiss, S. K., Yang, and S. N. Oh, 1994: A comparison of ERBE and AVHRR longwave flux estimates. *Bull. Amer. Meteor. Soc.*, **75**, 2115–2130.
- , and J. S. Winston, 1978: Earth-atmosphere radiative heating based on NOAA scanning radiometer measurements. *Bull. Amer. Meteor. Soc.*, **59**, 1570–1573.
- Gutzler, D. S., and T. M. Wood, 1990: Structure of large-scale convection anomalies over tropical oceans. *J. Climate*, **3**, 483–496.
- Harrison, E. F., D. R. Brooks, P. Minnis, B. A. Wielicki, W. F. Staylor, G. G. Gibson, D. F. Young, and F. M. Denn, 1988: First estimates of the diurnal variation of longwave radiation from the multiple-satellite Earth Radiation Budget Experiment (ERBE). *Bull. Amer. Meteor. Soc.*, **69**, 1144–1151.
- Hartmann, D. L., K. J. Kowalewski, and M. L. Michelsen, 1991: Diurnal variations of outgoing longwave radiation and albedo from ERBE scanner data. *J. Climate*, **4**, 598–618.
- Hendon, H. H., and M. L. Salby, 1994: The life cycle of the Madden and Julian Oscillation. *J. Atmos. Sci.*, **51**, 2225–2237.
- Hoel, P. G., 1984: *Introduction to Mathematical Statistics*. John Wiley and Sons, 593 pp.
- Hucek, R., L. Stowe, and R. Joyce, 1996: Evaluating the Design of an Earth Radiation Budget Instrument with System Simulations. Part III: CERES-I Diurnal Sampling Error. *J. Atmos. Oceanic Technol.*, **13**, 383–399.
- Jones, C., D. E. Waliser, and C. Gautier, 1998: The Influence of the Madden-Julian Oscillation on ocean surface heat fluxes and sea surface temperature variability in the warm pool region. *J. Climate*, **11**, 1057–1072.
- Kandel, R., and Coauthors, 1998: The ScaRaB Earth Radiation budget data set. *Bull. Amer. Meteor. Soc.*, **79**, 765–783.
- Kondragunta, C. R., and A. Gruber, 1995: Spurious semi-diurnal variation in the E.R.B.E. outgoing longwave radiation. NOAA Tech. Rep. NESDIS 84, 24 pp.
- Kyle, H. L., P. E. Ardanuy, and E. J. Hurley, 1985: The status of the Nimbus-7 Earth Radiation Budget dataset. *Bull. Amer. Meteor. Soc.*, **66**, 1378–1388.
- , and Coauthors, 1993: The Nimbus Earth Radiation Budget (ERB) experiment: 1975 to 1992. *Bull. Amer. Meteor. Soc.*, **74**, 815–830.
- Lau, K. M., and P. H. Chan, 1988: Intraseasonal and interannual variations of tropical convection: A possible link between the 40–50 day oscillation and ENSO? *J. Atmos. Sci.*, **36**, 437–457.
- Liebmann, B., and D. L. Hartmann, 1982: Interannual variations of outgoing IR associated with tropical circulation changes during 1974–78. *J. Atmos. Sci.*, **39**, 1153–1162.
- , and C. A. Smith, 1996: Description of a complete (interpolated) outgoing longwave radiation dataset. *Bull. Amer. Meteor. Soc.*, **77**, 1275–1277.
- Minnis, P., and Harrison E. F., 1984: Diurnal variability of regional cloud and clear-sky radiative parameters derived from GOES Data. 1. Analysis Method. *J. Climate Appl. Meteor.*, **23**, 993–1011.
- , D. F. Young, and E. F. Harrison, 1991: Examination of the relationship between outgoing infrared window and total longwave fluxes using satellite data. *J. Climate*, **4**, 1114–1136.
- Morrissey, M. L., 1986: A statistical analysis of the relationships among rainfall, outgoing longwave radiation, and the moisture budget during January–March 1979. *Mon. Wea. Rev.*, **114**, 931–942.
- , and N. E. Graham, 1996: Recent trends in rain gauge precipitation measurements from the tropical Pacific: Evidence for an enhanced hydrologic cycle. *Bull. Amer. Meteor. Soc.*, **77**, 1207–1219.
- Murakami, T., L. X. Chen, and A. Xie, 1979: Relationship among seasonal cycles, low-frequency oscillations, and transient disturbances revealed from outgoing longwave radiation data. *Mon. Wea. Rev.*, **118**, 1456–1465.
- Nitta, T., and S. Yamada, 1989: Recent warming of the tropical sea surface temperature and its relationship to the Northern Hemisphere circulation. *J. Meteor. Soc. Japan*, **67**, 375–383.
- NOAA Polar Orbiter Data User's Guide, 1998: K. B. Kidwell, Ed., U.S. Department of Commerce, Section 1–4.
- Preisendorfer, R. W., F. W. Zwiers, and T. P. Barnett, 1981: Foundations of principal component selection rules. Scripps Institution of Oceanography Rep. 81-7, 200 pp.
- Ramanathan, V., B. R. Barkstrom, and E. F. Harrison, 1989: Climate and the Earth's Radiation Budget. *Phys. Today*, **42**, 22–32.
- Rasmusson, E. M., and J. M. Wallace, 1983: Meteorological aspects of the El Niño/Southern Oscillation. *Science*, **222**, 1195–1202.
- Richman, M. B., 1986: Rotation of principal components. *J. Climate*, **6**, 293–335.
- , and W. E. Easterling, 1988: Procrustes Target Analysis: A multivariate tool for identification of climate fluctuations. *J. Geophys. Res.*, **93**, 10 989–11 003.
- Rieland, M., and E. Raschke, 1991: Diurnal variability of the Earth Radiation Budget—Sampling requirements, time integration aspects and error-estimates for the Earth Radiation Budget Experiment (ERBE). *Theor. Appl. Climatol.*, **44**, 9–24.
- Saunders, R. W., L. L. Stowe, G. E. Hunt, and C. F. England, 1983: An intercomparison between radiation budget estimates from METEOSAT 1, Nimbus 7 and TIROS-N satellites. *J. Climate Appl. Meteor.*, **22**, 546–559.
- Susskind, J., P. Piraino, L. Rokke, L. Iredell, and A. Mehta, 1997: Characteristics of the TOVS pathfinder Path A dataset. *Bull. Amer. Meteor. Soc.*, **78**, 1449–1472.
- Thomas, D., J. P. Duvel, and R. Kandel, 1995: Diurnal bias in calibration of broad-band radiance measurements from space. *IEEE Trans. Geosci. Remote Sens.*, **33**, 670–683.
- Trenberth, K. E., 1990: Recent observed interdecadal climate changes in the Northern Hemisphere. *Bull. Amer. Meteor. Soc.*, **71**, 988–993.

- , and T. J. Hoar, 1996: The 1990–95 El Niño–Southern Oscillation event: Longest on record. *Geophys. Res. Lett.*, **23**, 57–60.
- Vonder Haar, T. H., and V. E. Suomi, 1971: Measurements of the Earth's Radiation Budget from satellites during a five-year period. Part I: Extended Time and Space Means. *J. Atmos. Sci.*, **28**, 305–314.
- Waliser, D. E., and W. Zhou, 1997: Removing satellite equatorial crossing time biases from the OLR and HRC datasets. *J. Climate*, **10**, 2125–2146.
- , N. E. Graham, and C. Gautier, 1993: Comparison of the highly reflective cloud and outgoing longwave datasets for use in estimating tropical deep convection. *J. Climate*, **6**, 331–353.
- , C. Jones, J. K. Schemm, and N. E. Graham, 1999: A statistical extended-range tropical forecast model based on the slow evolution of the Madden–Julian Oscillation. *J. Climate*, **12**, 1918–1939.
- Wielicki, B. A., B. R. Barkstrom, E. F. Harrison, R. B. Lee III, G. L. Smith, and J. E. Cooper, 1996: Clouds and the Earth's Radiant Energy System (CERES): An Earth Observing System Experiment. *Bull. Amer. Meteor. Soc.*, **77**, 853–868.
- Xie, P., and P. A. Arkin, 1998: Global monthly precipitation estimates from satellite-observed outgoing longwave radiation. *J. Climate*, **11**, 137–164.
- Xie, P., J. E. Janowiak, P. A. Arkin, and S.-K. Yang, 2000: Diurnal variation of outgoing longwave radiation: Preliminary results based on harmonic analysis of the ERBS observations. Preprints, *10th Conf. on Satellite Meteorology and Oceanography*, Long Beach, CA, Amer. Meteor. Soc., 422–425.
- Yoo, J.-M., and J. A. Carton, 1988: Outgoing longwave radiation derived rainfall in the tropical Atlantic, with emphasis on 1983–84. *J. Climate*, **1**, 1047–1054.
- Young, D. F., P. Minnis, and D. R. Doelling, 1998: Temporal interpolation methods for the Clouds and the Earth's Radiant Energy system (CERES) experiment. *J. Appl. Meteor.*, **37**, 572–590.
- Zhang, M. H., R. D. Cess, and S. C. Xie, 1996: Relationship between cloud-radiative forcing and sea surface temperatures over the entire tropical oceans. *J. Climate*, **9**, 1374–1384.
- Zhang, Y.-C., W. B. Rossow, and A. A. Lacis, 1995: Calculation of surface and top of atmosphere radiative fluxes from physical quantities based on ISCCP datasets. 1. Method and sensitivity to input data uncertainties. *J. Geophys. Res.*, **100**, 1149–1165.